

Finite Element solution of the fiber/matrix interface crack problem: Convergence properties and mode mixity of the Virtual Crack Closure Technique

Luca Di Stasio^{a,b,*}, Zoubir Ayadi^b

^a Luleå University of Technology, University Campus, SE-97187, Luleå, Sweden

^b Université de Lorraine, EEIGM, IJL, 6 Rue Bastien Lepage, F-54010, Nancy, France

ARTICLE INFO

Keywords:

Fiber/matrix interface crack
Bi-material interface arc crack
Linear Elastic Fracture Mechanics (LEFM)
Virtual Crack Closure Technique (VCCT)
Mode separation
Convergence

ABSTRACT

The bi-material interface arc crack has been the focus of interest in the composite community, where it is usually referred to as the fiber-matrix interface crack. In this work, we investigate the convergence properties of the Virtual Crack Closure Technique (VCCT) when applied to the evaluation of the Mode I, Mode II and total Energy Release Rate of the fiber-matrix interface crack in the context of the Finite Element Method (FEM). We first propose a synthetic vectorial formulation of the VCCT. Thanks to this formulation, we study the convergence properties of the method, both analytically and numerically. It is found that Mode I and Mode II Energy Release Rate (ERR) possess a logarithmic dependency with respect to the size of the elements in the crack tip neighborhood, while the total ERR is independent of element size.

1. Introduction

Bi-material interfaces represent the basic load transfer mechanism at the heart of Fiber Reinforced Polymer Composite (FRPC) materials. They are present at the macroscale, in the form of adhesive joints; at the mesoscale, as interfaces between layers with different orientations; at the microscale, as fiber-matrix interfaces. Bi-material interfaces have for long attracted the attention of researchers in Fracture Mechanics [1,2], due to their hidden complexity.

The problem was first addressed in the 1950's by Williams [3], who derived through a linear elastic asymptotic analysis the stress distribution around an *open* crack (i.e. with crack faces nowhere in contact for any size of the crack) between two infinite half-planes of dissimilar materials. He found the existence of a strong oscillatory behavior in the stress singularity at the crack tip of the form

$$r^{-\frac{1}{2}} \sin(\varepsilon \log r) \quad \text{with} \quad \varepsilon = \frac{1}{2\pi} \log \left(\frac{1-\beta}{1+\beta} \right), \quad (1)$$

in both Mode I and Mode II. In Eq. (1), β is one of the two parameters introduced by Dundurs [4] to characterize bi-material interfaces:

$$\beta = \frac{\mu_2(\kappa_1 - 1) - \mu_1(\kappa_2 - 1)}{\mu_2(\kappa_1 + 1) + \mu_1(\kappa_2 + 1)} \quad (2)$$

where $\kappa = 3 - 4\nu$ in plane strain and $\kappa = \frac{3-4\nu}{1+\nu}$ in plane stress, μ is the shear modulus, ν Poisson's coefficient, and indexes 1, 2 refer to the two bulk materials joined at the interface. Defining a as the length of the crack, it was found that the size of the oscillatory region is in the order of $10^{-6}a$ [5]. Given the oscillatory behavior of the crack tip singularity of Eq. (1), the definition of Stress Intensity Factor (SIF) $\lim_{r \rightarrow 0} \sqrt{2\pi r} \sigma$ diverges and ceases to be valid [1]. It implies that the Mode mixity problem at the crack tip is ill-posed.

It was furthermore observed, always in the context of Linear Elastic Fracture Mechanics (LEFM), that an interpenetration zone exists close to the crack tip [6,7] with a length in the order of $10^{-4}a$ [6]. Following conclusions firstly proposed in Ref. [7], the presence of a *contact zone* in the crack tip neighborhood, of a length to be determined from the solution of the elastic problem, was introduced in Ref. [8] and shown to provide a physically consistent solution to the straight bi-material interface crack problem.

The curved bi-material interface crack, more often referred to as the fiber-matrix interface crack (or debond) due to its relevance in FRPCs, was first treated by England [9] and by Perlman and Sih [10], who provided the analytical solution of stress and displacement fields for a circular inclusion with respectively a single debond and an arbitrary number of debonds. Building on their work, Toya [11] particularized

* Corresponding author. Luleå University of Technology, University Campus, SE-97187, Luleå, Sweden.

E-mail address: luca.di.stasio@ltu.se (L. Di Stasio).

<https://doi.org/10.1016/j.finel.2019.103332>

Received 1 July 2019; Received in revised form 10 September 2019; Accepted 19 September 2019

Available online 4 October 2019

0168-874X/© 2019 Elsevier B.V. All rights reserved.

the solution and provided the expression of the Energy Release Rate (ERR) at the crack tip. The same problems exposed previously for the *open* straight bi-material crack were shown to exist also for the *open* fiber-matrix interface crack: the presence of strong oscillations in the crack tip singularity and onset of crack face interpenetration at a critical flaw size.¹

In order to treat cases more complex than the single partially debonded fiber in an infinite matrix of [9–11], numerical studies followed. In the 1990's, París and collaborators [12] developed a Boundary Element Method (BEM) with the use of discontinuous singular elements at the crack tip and the Virtual Crack Closure Integral (VCCI) [13] for the evaluation of the Energy Release Rate (ERR). They validated their results [12] with respect to Toya's analytical solution [11] and analyzed the effect of BEM interface discretization on the stress field in the neighborhood of the crack tip [14]. Following Comninou's work on the straight crack [8], they furthermore recognized the importance of contact to retrieve a physical solution avoiding interpenetration [12] and studied the effect of the contact zone on debond ERR [15]. Their algorithm was then applied to investigate the fiber-matrix interface crack under different geometrical configurations and mechanical loadings [16–22].

Recently the Finite Element Method (FEM) was also applied to the solution of the fiber-matrix interface crack problem [23–25], in conjunction with the Virtual Crack Closure Technique (VCCT) [26,27] for the evaluation of the ERR at the crack tip. In Ref. [23], the authors validated their model with respect to the BEM results of [12], but no analysis of the effect of the discretization in the crack tip neighborhood comparable to Ref. [14] was proposed. Thanks to the interest in evaluating the ERR of interlaminar delamination, different studies exist in the literature on the effect of mesh discretization on Mode I and Mode II ERR of the straight bi-material interface crack when evaluated with the VCCT in the context of the FEM (see for example [28] for a review). An early result on the problem is available in Ref. [29]. Here the authors evaluated with the Virtual Crack Closure Technique Mode I and Mode II Energy Release Rate of both a central crack and an edge crack at the interface between two 2D plates of different isotropic materials subjected to tensile loading. They showed analytically that the total ERR G is well defined while Mode I and Mode II ERR, respectively G_I and G_{II} , do not converge. They confirmed their analytical derivations numerically by solving the two problems with the Finite Element Method and evaluating the ERR with the VCCT. Referring to the crack length as a and to the length of an element at the crack tip as Δa , they found that the total ERR was independent of normalized element size $\Delta a/a$ while G_I and G_{II} were dependent on assumed crack extension, i.e. element size at the crack tip. In particular, they showed a decreasing G_I and an increasing G_{II} with decreasing element size for both crack configurations. The same analysis was conducted, and analogous results obtained, in Ref. [30] for a central crack under either far-field tensile or shear loading between two orthotropic materials in 2D and in Ref. [31] for a central crack subjected to far-field tension between two orthotropic solids in 3D. The convergence of VCCT-based mode decomposition was analyzed in Ref. [32] for edge delaminations in laminated composites subjected to tensile loading coplanar and normal to crack propagation direction in a quasi-3D setting. Again, it was observed that the total ERR was independent of mesh size while Mode I and Mode II ERR showed dependency and no convergence could be established. In this configuration however, it was found that G_I increases and G_{II} decreases with decreasing element size. The application of the VCCT to the problem of composite skin-stiffener debonding was considered in Ref. [33] in conjunction with 2D plate elements, where the authors studied the effect of different combinations of adherends' layout, thick-

ness and fiber orientation at the interface on Mode decomposition. Only in the case of skin and stiffener with the same layout, same thickness and identical fiber orientation at the interface, Mode I and Mode II were found to be independent of mesh size. In all other cases, G_I and G_{II} were dependent on assumed crack extension and showed a trend similar to the one in Ref. [32]. The absence of a converging Mode-decomposed solution with the VCCT has motivated proposals for alternative solution. In Ref. [34], the authors analyze several proposals of mode-mixity parameters and suggest a correction to the VCCT-based mode-mixity ratio by assuming a reference characteristic length. The authors themselves however admit that this characteristic length has no physical interpretation. In Ref. [35], the problem of Mode-decomposition is solved through the development of analytical relations based on Euler and Timoshenko beam models. It is however well suited only for those configurations that can be split into beam elements, such as the Double Cantilever Beam (DCB) specimen.

No comparable analysis can be found in the literature on Mode separation and convergence analysis of the VCCT when applied to the fiber-matrix interface crack (circular bi-material interface crack) problem in the context of a linear elastic FEM solution. In the present article, we first present the FEM formulation of the problem, together with the main geometrical characteristics, material properties, boundary conditions and loading. We then propose a vectorial formulation of the VCCT and express Mode I and Mode II ERR in terms of FEM natural variables. Differently from the usual approach found in the literature, we do not express G_I and G_{II} as functions of stress and displacement fields using the results from complex analysis. We instead focus on the mathematical structure of the 1-step VCCT in the context of the Finite Element Method and write the crack tip forces as a linear combination of the crack faces displacements at the crack tip (plus a term representing the influence of the rest of the model). The ERR is consequently a quadratic function of the crack faces displacements. Given that, if the FEM solution is converging, stress and displacement fields are characterized by the oscillating singularity of Equation (1), it is possible to evaluate the behavior of the VCCT-calculated Energy Release Rate in the limit of crack tip element size going to zero. We are thus able to derive analytically a functional form of the dependency of the ERR on crack tip element size. Finally, the functional form thus derived is compared to the numerical results obtained with the Finite Element Method.

2. FEM formulation of the fiber-matrix interface crack problem

In order to investigate the fiber-matrix interface crack problem, a 2-dimensional model of a single fiber inserted in a rectangular matrix element is considered (see Fig. 1). Total element length and height are respectively $2L$ and L , where L is determined by the fiber radius R_f and the fiber volume fraction V_f by

$$L = \frac{R_f}{2} \sqrt{\frac{\pi}{V_f}}. \quad (3)$$

The fiber radius R_f is assumed to be equal to 1 μm . This choice is not dictated by physical considerations but for simplicity. It is thus useful to remark that, in a linear elastic solution as the one considered in the present work, the ERR is proportional to the geometrical dimensions of the model and, consequently, recalculation of the ERR for fibers of any size requires a simple multiplication.

As shown in Fig. 1, the debond is placed symmetrically with respect to the x axis and its size is characterized by the angle $\Delta\theta$ (which makes the full debond size equal to $2\Delta\theta$ and the full crack length equal to $R_f 2\Delta\theta$). A region $\Delta\Phi$ of unknown size appears at the crack tip for large debond sizes (at least $\geq 60^\circ$ – 80°), in which the crack faces are in contact with each other and free to slide. Frictionless contact is thus considered between the two crack faces to allow free sliding and avoid interpenetration. Symmetry with respect to the x axis is applied on the lower boundary while the upper surface is left free. Kinematic coupling on the x -displacement is applied along the left and right sides of the model

¹ For the fiber-matrix interface crack, flaw size is measured in terms of the angle $\Delta\theta$ subtended by half of the arc-crack, i.e. $a = 2\Delta\theta R_f$ where R_f is the inclusion (fiber) radius and $\Delta\theta$ is expressed in radians.

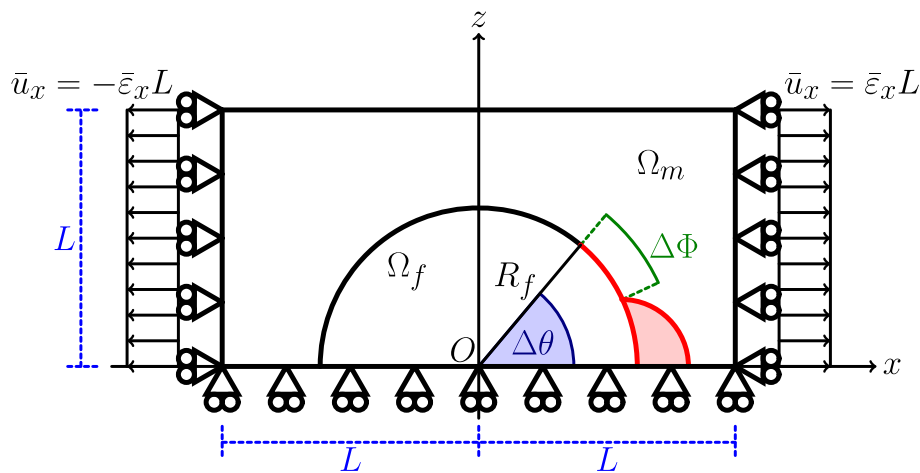


Fig. 1. Schematic of the model with its main parameters.

Table 1

Summary of the mechanical properties of fiber and matrix. E stands for Young's modulus, μ for shear modulus and ν for Poisson's ratio.

Material	E [GPa]	μ [GPa]	ν [—]
Glass fiber	70.0	29.2	0.2
Epoxy	3.5	1.25	0.4

in the form of a constant x -displacement $\pm \bar{\epsilon}_x L$, which corresponds to transverse strain $\bar{\epsilon}_y$ equal to 1% in the results here presented.

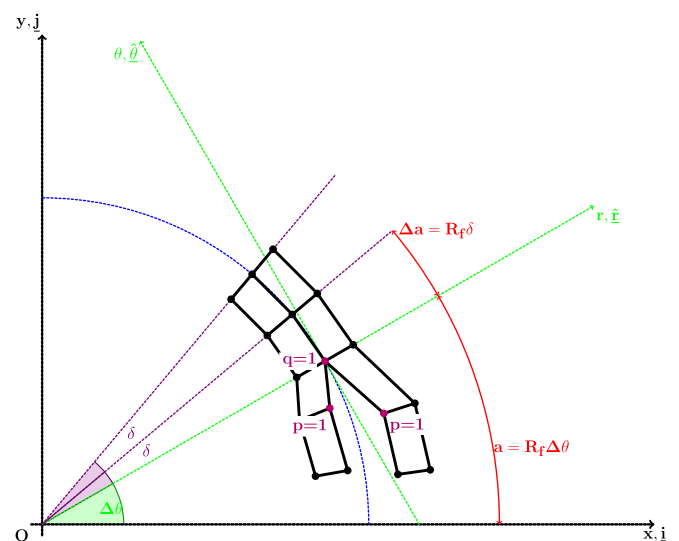
The model problem is solved with the Finite Element Method (FEM) within the Abaqus environment, a commercial FEM software [36]. The model is meshed with second order, 2D, plane strain triangular (CPE6) and rectangular (CPE8) elements. A regular mesh of rectangular elements with almost unitary aspect ratio is used at the crack tip. The angular size δ of an element in the crack tip neighborhood represents the main parameter of the numerical analysis. The crack faces are modeled as element-based surfaces and a small-sliding contact pair interaction with no friction is imposed between them. The Mode I, Mode II and total Energy Release Rates (ERRs) (respectively referred to as G_I , G_{II} and G_{TOT}) are evaluated using the VCCT [27], implemented in a in-house Python routine. A glass fiber-epoxy system is considered in the present work, and it is assumed that their response lies always in the linear elastic domain. The elastic properties of glass fiber and epoxy are reported in Table 1.

3. Vectorial formulation of the Virtual Crack Closure Technique (VCCT)

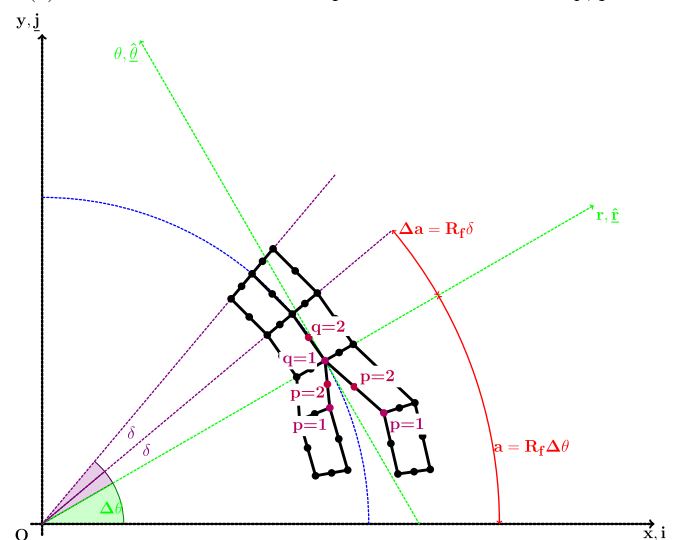
In order to express the VCCT formulation of the ERR in terms of FEM variables, we need to introduce a few rotation matrices in order to represent the discretized representation (FE mesh) of a crack along a circular interface. The position of the crack tip is characterized by the angular size of the crack (see Sec. 2 and Fig. 1 for reference) and the rotation corresponding to the crack tip reference frame is represented by the matrix $\mathbf{R}_{\Delta\theta}$ defined as

$$\underline{R}_{\Delta\theta} = \begin{bmatrix} \cos(\Delta\theta) & \sin(\Delta\theta) \\ -\sin(\Delta\theta) & \cos(\Delta\theta) \end{bmatrix}. \quad (4)$$

Nodes belonging to the elements sharing the crack tip are involved in the VCCT estimation of the ERR and it is assumed that, given a sufficiently fine discretization, they are aligned with the crack propagation

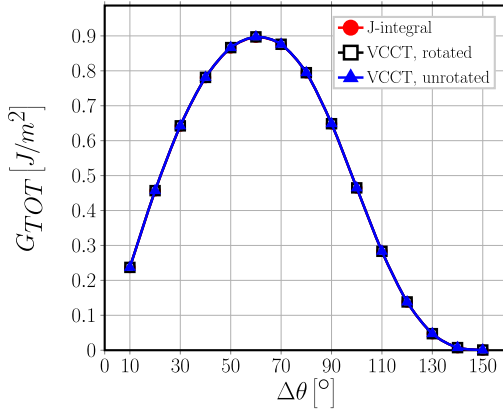


(a) Elements with 1^{st} order shape functions: $m = 1$ and $p, q = 1$.

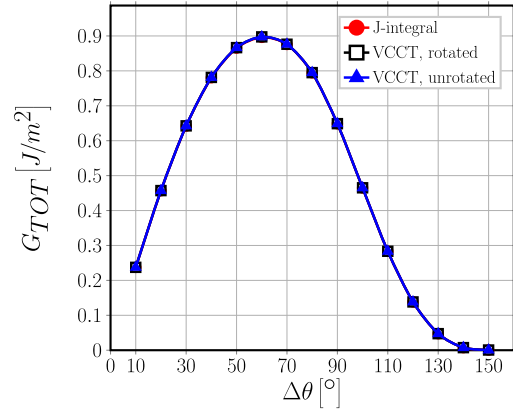


(b) Elements with 2^{nd} order shape functions: $m = 2$ and $p, q = 1, 2$.

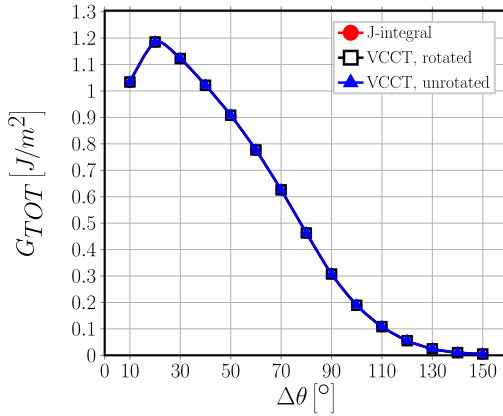
Fig. 2. Schematic of the mesh at the fiber/matrix interface crack tip.



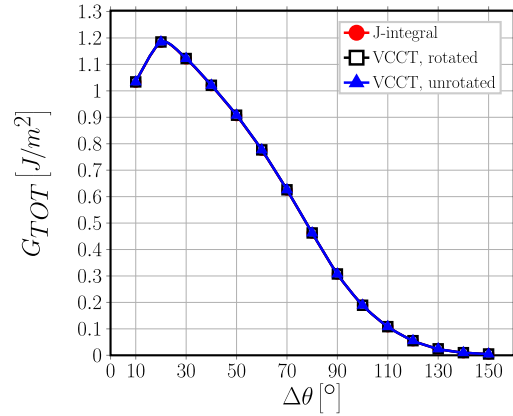
(a) $V_f = 0.1\%$, 1^{st} order elements, $\delta = 0.05^\circ$.



(b) $V_f = 0.1\%$, 2^{nd} order elements, $\delta = 0.05^\circ$.



(c) $V_f = 40\%$, 1^{st} order elements, $\delta = 0.05^\circ$.



(d) $V_f = 40\%$, 2^{nd} order elements, $\delta = 0.05^\circ$.

Fig. 3. Numerical invariance of the total Energy Release Rate: G_{TOT} computed with the VCCT with rotated forces and displacements (label *rotated*), with the VCCT with forces and displacements in the global reference frame (label *unrotated*) and with J-integral method (label *J-integral*).

direction defined at the crack tip.

However, irrespectively of how small the elements in the crack tip neighborhood are, a misalignment always exists with respect to the assumed crack propagation direction (in the crack tip reference frame). This is measured by the matrices $\underline{\underline{P}}_\pi(p)$, defined as

$$\underline{\underline{P}}_\pi(p) = \begin{bmatrix} \cos\left(\left(1 + \frac{1-p}{m}\right)\delta\right) & \sin\left(\left(1 + \frac{1-p}{m}\right)\delta\right) \\ -\sin\left(\left(1 + \frac{1-p}{m}\right)\delta\right) & \cos\left(\left(1 + \frac{1-p}{m}\right)\delta\right) \end{bmatrix} \quad (5)$$

and $\underline{\underline{Q}}_\delta(q)$, equal to

$$\underline{\underline{Q}}_\delta(q) = \begin{bmatrix} \cos\left(\frac{q-1}{m}\delta\right) & \sin\left(\frac{q-1}{m}\delta\right) \\ -\sin\left(\frac{q-1}{m}\delta\right) & \cos\left(\frac{q-1}{m}\delta\right) \end{bmatrix}, \quad (6)$$

respectively for the free and bonded nodes involved in the VCCT estimation. In Eqs. (5) and (6), δ is the angular size of an element in the crack tip neighborhood (see Sec. 2 and Fig. 1), m is the order of the element shape functions and $p, q = 1, \dots, m$ are indices referring to the nodes belonging respectively to free and bonded elements sharing the crack tip. Fig. 2 shows the p, q -based numbering of nodes at the crack

tip in the case of elements with linear and quadratic (serendipity) shape functions. Introducing the permutation matrix

$$\underline{\underline{P}}_\pi = \begin{bmatrix} 0 & 1 \\ -1 & 0 \end{bmatrix}, \quad (7)$$

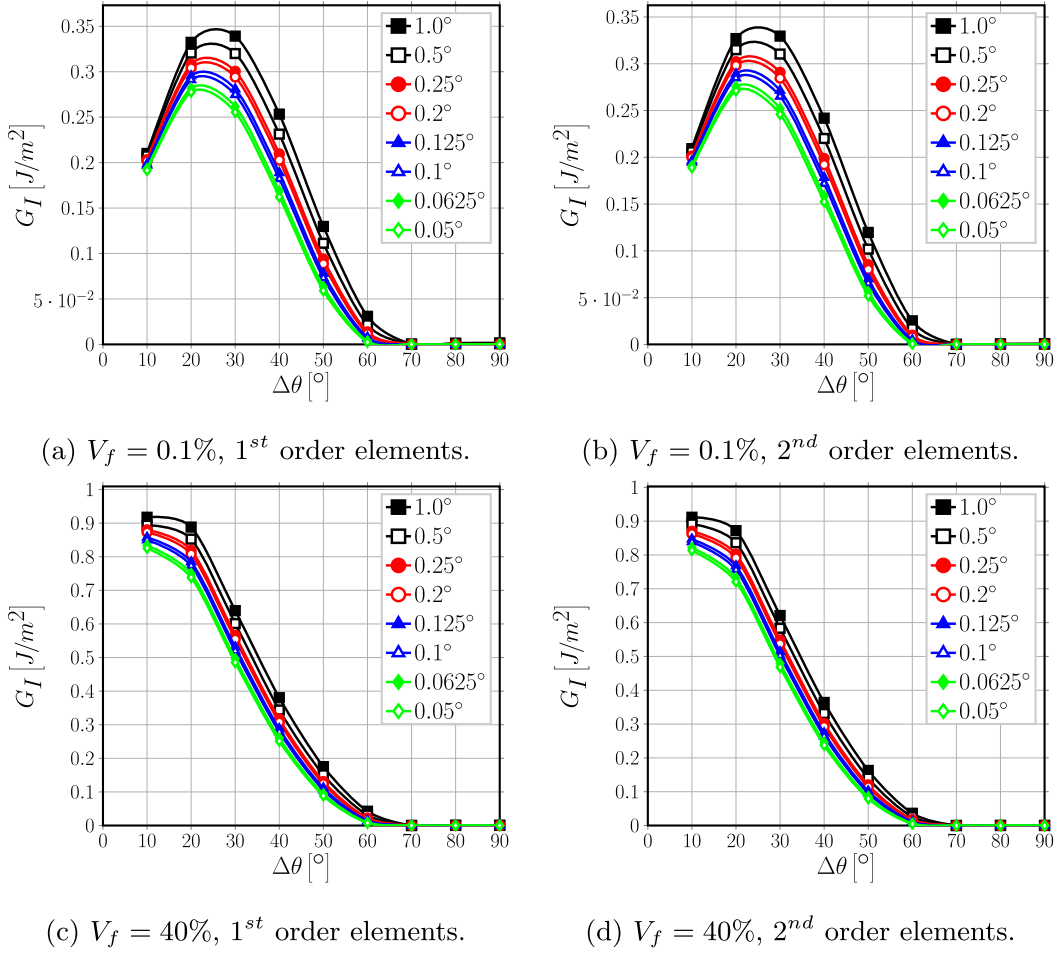
it is possible to express the derivatives of rotation matrices $\underline{\underline{R}}_{\Delta\theta}$, $\underline{\underline{P}}_\pi$ and $\underline{\underline{Q}}_\delta$ with respect to their argument:

$$\frac{\partial \underline{\underline{R}}_{\Delta\theta}}{\partial \Delta\theta} = \underline{\underline{P}}_\pi \cdot \underline{\underline{R}}_{\Delta\theta}, \quad \frac{\partial \underline{\underline{P}}_\pi}{\partial \delta} = \left(1 + \frac{1-p}{m}\right) \underline{\underline{P}}_\pi \cdot \underline{\underline{P}}_\pi,$$

$$\frac{\partial \underline{\underline{Q}}_\delta}{\partial \delta} = \frac{q-1}{m} \underline{\underline{P}}_\pi \cdot \underline{\underline{Q}}_\delta. \quad (8)$$

By means of Eqs. (5) and (6), we can express the crack tip forces $\underline{\underline{F}}_{xy} = \begin{bmatrix} F_x \\ F_y \end{bmatrix}$ and crack displacements $\underline{\underline{u}}_{xy} = \begin{bmatrix} u_x \\ u_y \end{bmatrix}$ in the crack tip reference frame (where the tangential direction θ correspond to the direction of crack propagation) while taking into account the misalignment to the finite discretization as

$$\underline{\underline{F}}_{r\theta} = \underline{\underline{Q}}_\delta \underline{\underline{R}}_{\Delta\theta} \underline{\underline{F}}_{xy}, \quad \underline{\underline{u}}_{r\theta} = \underline{\underline{P}}_\pi \underline{\underline{R}}_{\Delta\theta} \underline{\underline{u}}_{xy} \quad (9)$$

Fig. 4. Effect of the size δ of an element at the crack tip on Mode I ERR.

where $\underline{F}_{r\theta} = \begin{bmatrix} F_r \\ F_\theta \end{bmatrix}$ and $\underline{u}_\theta = \begin{bmatrix} u_r \\ u_\theta \end{bmatrix}$.

The crack tip forces can be expressed as a function of the crack opening displacement as

$$\underline{F}_{xy} = \underline{K}_{xy} \underline{u}_{xy} + \tilde{\underline{F}}_{xy}, \quad (10)$$

where \underline{K}_{xy} is in general a full matrix of the form $\underline{K}_{xy} = \begin{bmatrix} K_{xx} & K_{xy} \\ K_{yx} & K_{yy} \end{bmatrix}$ and $\tilde{\underline{F}}_{xy}$ represents the effect of the rest of the FE solution through the remaining nodes of the elements attached to the crack tip. As such, the term $\tilde{\underline{F}}_{xy}$ can be expressed as a linear combination of the solution vector \underline{u}_N of nodal displacements of the form $\tilde{\underline{K}}_N \underline{u}_N$. Equation (10) thus become

$$\underline{F}_{xy} = \underline{K}_{xy} \underline{u}_{xy} + \tilde{\underline{K}}_N \underline{u}_N. \quad (11)$$

An exemplifying derivation of the relationships expressed in Equations (10) and (11) can be found in Appendix A. It is worthwhile to observe that another author [37,38] proposes a similar relationship, but in terms of flexibility $\underline{u} = \underline{CF}$. In Refs. [37,38], Valvo expresses the forces at the crack tip as a (linear) function of the crack faces displacements at the same point. The technique analyzed in Refs. [37,38] is the 2-steps VCCT [27]: given a structure with a crack of length a , a first simulation is run to compute the forces at the crack tip and, in the case, at the internal nodes of the first bonded element for p -refined meshes; then, a second simulation is conducted with the crack extended by Δa , where in practice Δa is the length of the element at the crack

tip, and crack faces displacements are evaluated at the same nodes, now released, where previously forces were extracted. The Energy Release Rate is computed as the product of forces and displacements evaluated at the same nodes. The 2-steps VCCT adheres more strictly to the principle of the crack closure integral [13,39]: the work needed to open the crack by δa (Energy Release Rate) is equal in magnitude to the work required to close it by the same amount. Forces and displacements should be thus evaluated at the same point respectively in the closed and open crack configuration. In this paper, we consider on the other hand the 1-step VCCT [27]: if the size of the elements at the crack tip is sufficiently small, the error committed by approximating the crack faces displacements at the crack tip with those one element before is negligible. This in turn eliminates the need for a second simulation and thus cut the required computational time by a half. Following the principle of the crack closure integral [13,39], Valvo's proposal is based on the observation that the crack face displacements at the crack tip for a virtual crack extension will be equal in magnitude and opposite in sign due the displacements caused by the application of crack tip forces. Thus, namely: $u_{open\ crack} = -u_{closed\ crack} = f(F_{closed\ crack})$, and for linear elastic materials $f(F_{closed\ crack})$ would be linear, hence the introduction of a flexibility matrix [38]. Given that we instead work with the 1-step VCCT, we start from the observation that, in a Finite Element solution, the forces at a point can be expressed as a linear combination of all the displacements of the model through the global stiffness matrix. We have followed a stiffness approach and we have proceeded to isolate the contribution of crack faces displacements on crack tip forces. This leaves an additional term $\tilde{\underline{K}}_N \underline{u}_N$ in Equation (11), which represents the contribution of the rest of the model and that is not present in Valvo's

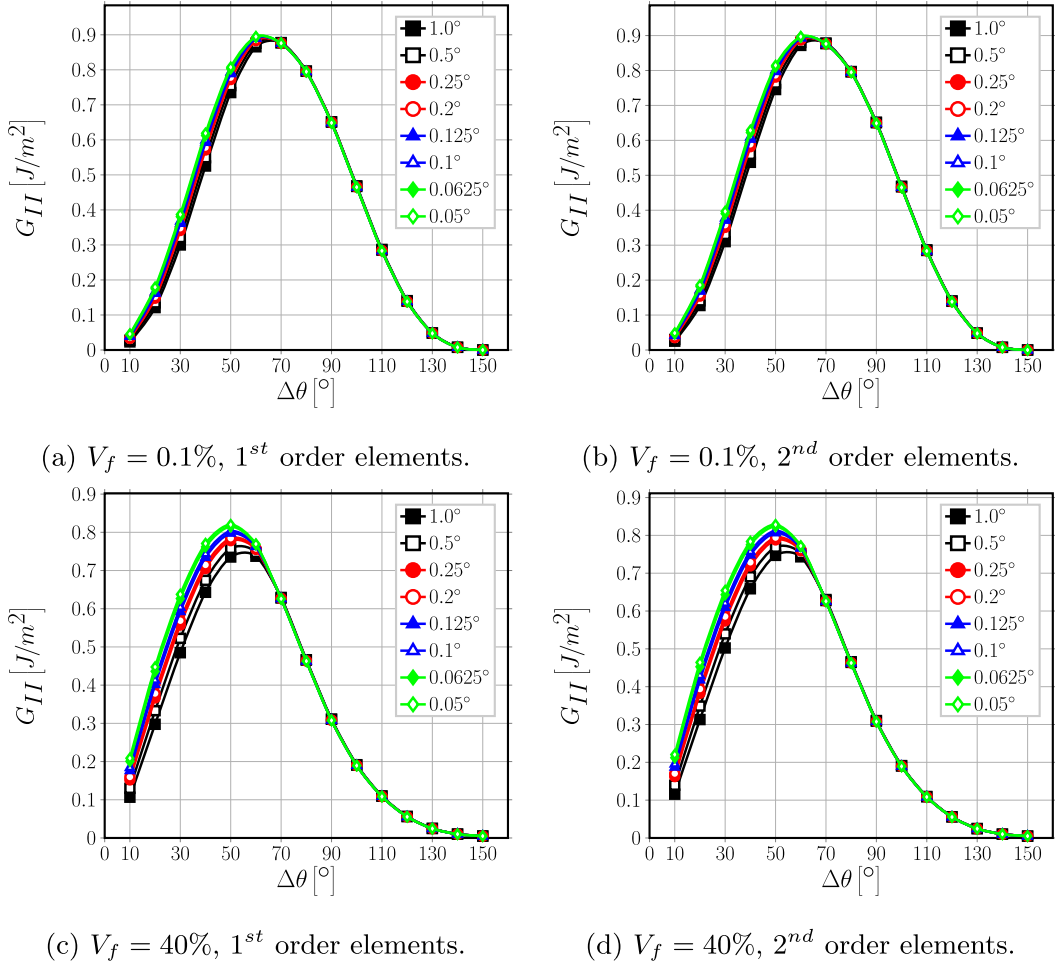


Fig. 5. Effect of the size δ of an element at the crack tip on Mode II ERR.

proposal. Notice that the linearity of Equation (11) does not stem from material linearity, but from the structure of the FEM solution. It can thus, in principle, be applied to non-linear materials, although as part of a secant- or tangent-based linearization. Notice that both the stiffness matrix of Equation (11) and Valvo's flexibility matrix possess out-of-diagonal elements, which represent the contribution of Poisson's effect.

Based upon the work of Raju [40], we introduce the matrix \underline{T}_{pq} to represent the weights needed in the VCCT to account for the use of singular elements. As already done previously, indices p and q refer to nodes placed respectively on the free (crack face) and bonded side of the crack tip. Nodes are enumerated so that the crack tip has always index 1, i.e. the higher the index the further the node is from the crack tip. Matrix \underline{T}_{pq} has always a size of $d \times d$, where $d = 2$ for a 2D problem and $d = 3$ for a 3D problem. An element $\underline{T}_{pq}(i, j)$ with $i, j = 1, \dots, d$ represents the weight to be assigned to the product of component i of the displacement extracted at node p with component j of the force extracted at node q . The expression of \underline{T}_{pq} for quadrilateral elements with or without singularity is reported in Appendix B. Notice that, given m is the order of the element shape functions, the element side has $m+1$ nodes and this represents the upper limit of indices p and q .

By using matrix \underline{T}_{pq} , it is possible to express the total ERR G evaluated with the VCCT as

$$G_{TOT} = \frac{1}{2R_f\delta} \sum_{p=1}^{m+1} \sum_{q=1}^{m+1} Tr \left(\underline{F}_{r\theta,q} \underline{u}_{r\theta,p}^T \underline{T}_{pq}^T \right), \quad (12)$$

where the symbol Tr stands for the *Trace* operator, which sums together the elements on the matrix main diagonal (first matrix invariant). Introducing the vector $\underline{G} = \begin{bmatrix} G_I \\ G_{II} \end{bmatrix}$ of fracture mode ERRs, Mode I and Mode II ERR evaluated with the VCCT can be expressed as

$$\underline{G} = \frac{1}{2R_f\delta} \sum_{p=1}^{m+1} \sum_{q=1}^{m+1} Diag \left(\underline{F}_{r\theta,q} \underline{u}_{r\theta,p}^T \underline{T}_{pq}^T \right), \quad (13)$$

where $Diag()$ is the function that extracts the main diagonal of the input matrix as a column vector. Substituting Equations (9) and (11) in Equations (12) and (13), we can express the Mode I, Mode II and total Energy Release Rate as a function of the crack displacements and the FE solution (more details in Appendix A) as

$$G_{TOT} = \frac{1}{2R_f\delta} \sum_{p=1}^{m+1} \sum_{q=1}^{m+1} Tr \left(\underline{Q}_{\Delta\theta} \underline{R}_{\Delta\theta} \underline{K}_{xy,q} \underline{u}_{xy,q}^T \underline{R}_{\Delta\theta}^T \underline{P}_{\Delta\theta}^T \underline{T}_{pq}^T \right) + \frac{1}{2R_f\delta} \sum_{p=1}^{m+1} \sum_{q=1}^{m+1} Tr \left(\underline{Q}_{\Delta\theta} \underline{R}_{\Delta\theta} \underline{\tilde{K}}_{xy,q} \underline{u}_{xy,q}^T \underline{R}_{\Delta\theta}^T \underline{P}_{\Delta\theta}^T \underline{T}_{pq}^T \right) \quad (14)$$

and

$$\underline{G} = \begin{bmatrix} G_I \\ G_{II} \end{bmatrix} = \frac{1}{2R_f\delta} \sum_{p=1}^{m+1} \sum_{q=1}^{m+1} Diag \left(\underline{Q}_{\Delta\theta} \underline{R}_{\Delta\theta} \underline{K}_{xy,q} \underline{u}_{xy,q}^T \underline{R}_{\Delta\theta}^T \underline{P}_{\Delta\theta}^T \underline{T}_{pq}^T \right) + \frac{1}{2R_f\delta} \sum_{p=1}^{m+1} \sum_{q=1}^{m+1} Diag \left(\underline{Q}_{\Delta\theta} \underline{R}_{\Delta\theta} \underline{\tilde{K}}_{xy,q} \underline{u}_{xy,q}^T \underline{R}_{\Delta\theta}^T \underline{P}_{\Delta\theta}^T \underline{T}_{pq}^T \right) \quad (15)$$

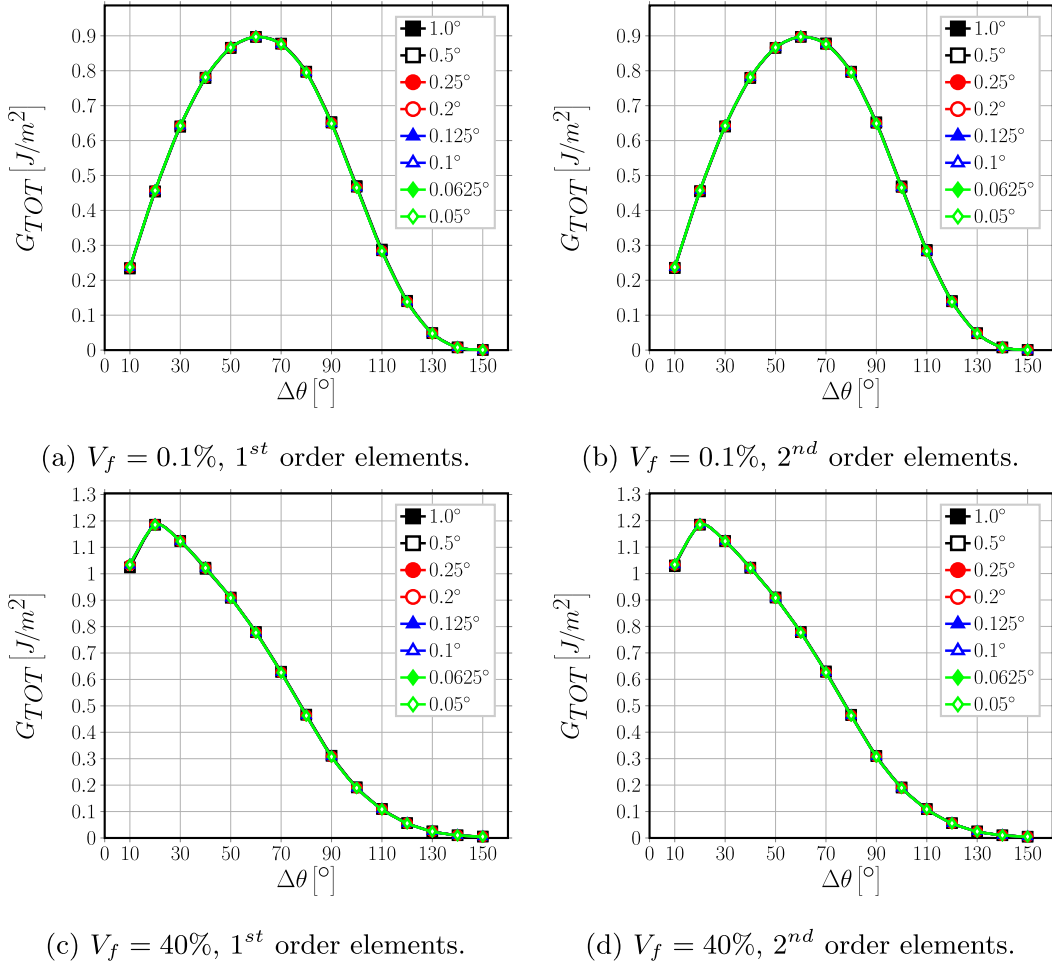


Fig. 6. Effect of the size δ of an element at the crack tip on total ERR.

Notice that the matrix appearing in Equation (14) and Equation (15) has the dimension of ERR, i.e. J/m^2 , and is in general full. Equation (14) states that the total Energy Release Rate is the first invariant of the matrix, i.e. its trace. Equation (15) states on the other hand that the elements on its diagonal are the Mode I and Mode II ERR. The off-diagonal components represent an interaction Energy Release Rate, mention of which can be already found in Ref. [41]. However, in Ref. [41] the existence of the interaction ERR is assumed based on physical assumptions, here it is derived from the mathematical structure of the VCCT in the context of the Finite Element Method. Valvo [37,38] derives as well the existence of an interaction ERR from the presence of non-zero off-diagonal elements in his flexibility matrix. He then considers that correct Mode-decomposition is provided when the off-diagonal terms are zero and thus derives a correction to the VCCT. A different perspective is offered here. Dimensional analysis suggests that the Energy Release Rate (J/m^2), i.e. the energy required to cause a unit increase in the crack surface size, is dimensionally equivalent to the Crack Driving Force (N/m), which is the force required to grow the crack along its path by a unit length. It is then possible to infer a physical interpretation of the elements of the ERR matrix of Equation (14) and Equation (15): the diagonal elements are respectively the Mode I (Mode II) force required to propagate the crack by a unit length in Mode I (Mode II); the off-diagonal elements are respectively the Mode I (Mode II) force required to propagate the crack by a unit length in Mode II (Mode I). The off-diagonal elements capture an interaction due to Poisson's effect and the mismatch of elastic properties between phases that is peculiar of bi-material interface cracks. The assumption by Valvo

[37,38] that correct Mode-decomposition is recovered by imposing that off-diagonal elements be equal to zero seems thus open to further reflection. A deeper analysis of this issue is however beyond the scope of this paper and it will be left to a future work.

4. Rotational invariance of G_{TOT}

Recalling Equation (14) and observing that matrix \underline{T}_{pq} is always equal to the identity matrix pre-multiplied by a suitable real constant (see Eq. (B.1) in Appendix B), the total Energy Release Rate can be rewritten as

$$\begin{aligned}
 G_{TOT} &= \frac{1}{2R_f\delta} \sum_{p=1}^{m+1} \sum_{q=1}^{m+1} Tr \\
 &\times \left(\underline{Q}_{\underline{\delta}=\Delta\theta} \underline{R}_{\underline{\delta}=\Delta\theta} \left(\underline{K}_{xy,q} \underline{u}_{xy,q} + \tilde{\underline{F}}_{xy,q} \right) \underline{u}_{xy,p}^T \underline{T}_{pq}^T \underline{R}_{\underline{\delta}=\Delta\theta}^T \underline{P}_{\underline{\delta}=\Delta\theta}^T \right) \\
 &= \frac{1}{2R_f\delta} \sum_{p=1}^{m+1} \sum_{q=1}^{m+1} Tr \left(\underline{Q}_{\underline{\delta}=\Delta\theta} \underline{R}_{\underline{\delta}=\Delta\theta} \underline{F}_{xy,q} \underline{u}_{xy,p}^T \underline{T}_{pq}^T \underline{R}_{\underline{\delta}=\Delta\theta}^T \underline{P}_{\underline{\delta}=\Delta\theta}^T \right),
 \end{aligned} \quad (16)$$

where \underline{F}_{xy} and \underline{u}_{xy} are the vectors of respectively the crack tip forces and crack displacements in the global ($x - y$) reference frame. Given that $\underline{Q}_{\underline{\delta}=\Delta\theta}$, $\underline{P}_{\underline{\delta}=\Delta\theta}$ and $\underline{R}_{\underline{\delta}=\Delta\theta}$ all represent a linear transformation (a rigid rotation in particular), the invariance of the trace to linear transformations ensures

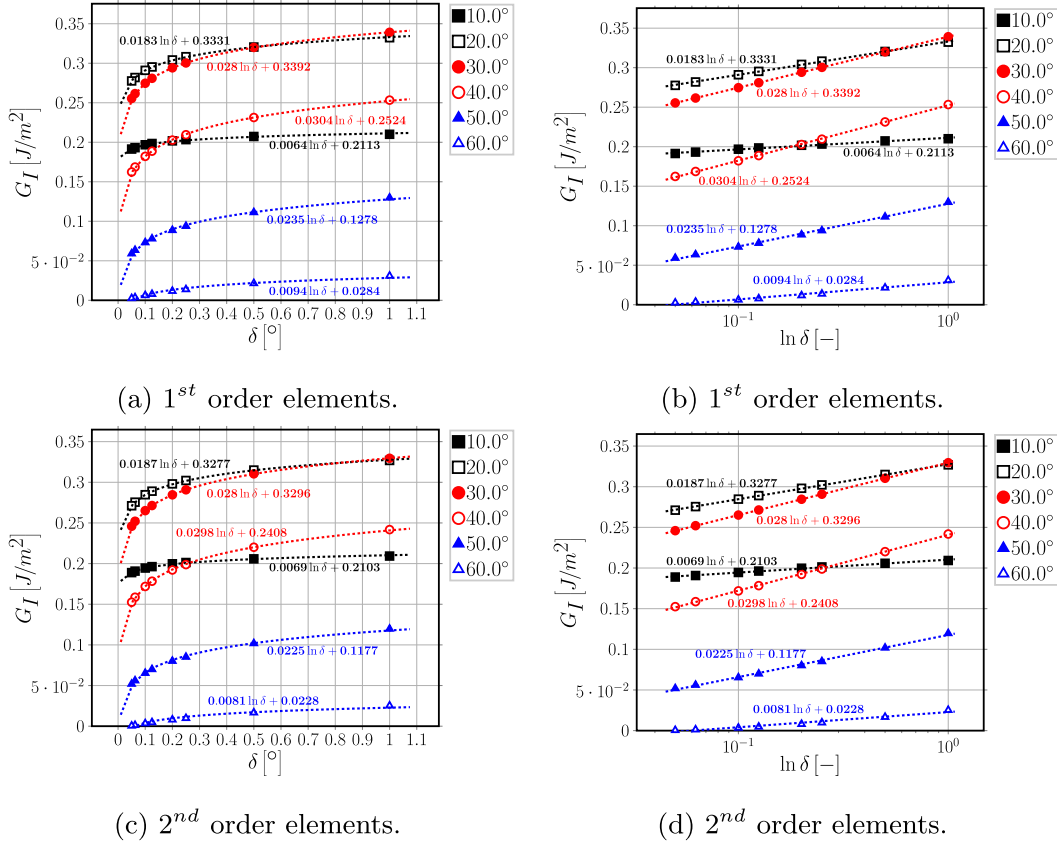


Fig. 7. Logarithmic dependence on δ of Mode I ERR: interpolation of numerical results for $V_f = 0.1\%$.

that

$$G_{TOT} = \frac{1}{2R_f\delta} \sum_{p=1}^{m+1} \sum_{q=1}^{m+1} \text{Tr} \left(\underline{\underline{Q}}_{\Delta\theta} \underline{\underline{R}}_{\Delta\theta} \underline{\underline{F}}_{xy,q} \underline{\underline{u}}_{xy,p}^T \underline{\underline{T}}_{pq}^T \underline{\underline{R}}_{\Delta\theta}^T \underline{\underline{P}}_{pq}^T \right) =$$

$$= \frac{1}{2R_f\delta} \sum_{p=1}^{m+1} \sum_{q=1}^{m+1} \text{Tr} \left(\underline{\underline{F}}_{xy,q} \underline{\underline{u}}_{xy,p}^T \underline{\underline{T}}_{pq}^T \right). \quad (17)$$

As G_{TOT} was defined according to Equation (12) and given that $\text{Tr}(AB) = \text{Tr}(BA)$, it holds that

$$G_{TOT} = \frac{1}{2R_f\delta} \sum_{p=1}^{m+1} \sum_{q=1}^{m+1} \underline{\underline{u}}_{r\theta,p}^T \underline{\underline{T}}_{pq}^T \underline{\underline{F}}_{r\theta,q}$$

$$= \frac{1}{2R_f\delta} \sum_{p=1}^{m+1} \sum_{q=1}^{m+1} \text{Tr} \left(\underline{\underline{F}}_{r\theta,q} \underline{\underline{u}}_{r\theta,p}^T \underline{\underline{T}}_{pq}^T \right)$$

$$= \frac{1}{2R_f\delta} \sum_{p=1}^{m+1} \sum_{q=1}^{m+1} \text{Tr} \left(\underline{\underline{F}}_{xy,q} \underline{\underline{u}}_{xy,p}^T \underline{\underline{T}}_{pq}^T \right)$$

$$= \frac{1}{2R_f\delta} \sum_{p=1}^{m+1} \sum_{q=1}^{m+1} \underline{\underline{u}}_{xy,p}^T \underline{\underline{T}}_{pq}^T \underline{\underline{F}}_{xy,q} \quad (18)$$

which shows that the total Energy Release Rate is invariant to rigid rotations and can be calculated equivalently with forces and displacements expressed in the local crack tip reference frame or the global reference frame. The analytical result is confirmed by the numerical solution of the fiber-matrix interface crack with different element orders and model fiber volume fractions, as shown in Fig. 3.

The result of Equation (18) has also physical implications:

- given that stress and displacement fields at the crack tip are the same, two cracks with different crack paths are energeti-

cally equivalent with respect to the total Energy Release Rate; – given that laws of the type $G_{TOT} \geq G_c$ govern crack propagation, if G_c do not depend on mode ratio, crack orientation will not affect its growth.

5. Convergence analysis

5.1. Analytical considerations

Substituting Equation (8) in the derivative of Equation (13), we can investigate the dependency of Mode I and Mode II ERR with respect to the size δ of an element in the crack tip neighborhood through

$$\frac{\partial G}{\partial \delta} = -\frac{1}{2R_f\delta^2} \sum_{p=1}^{m+1} \sum_{q=1}^{m+1} \text{Diag} \left(\underline{\underline{Q}}_{\Delta\theta} \underline{\underline{R}}_{\Delta\theta} \underline{\underline{K}}_{xy} \underline{\underline{u}}_{xy} \underline{\underline{u}}_{xy}^T \underline{\underline{R}}_{\Delta\theta}^T \underline{\underline{P}}_{pq}^T \underline{\underline{T}}_{pq}^T \right)$$

$$- \frac{1}{2R_f\delta^2} \sum_{p=1}^{m+1} \sum_{q=1}^{m+1} \text{Diag} \left(\underline{\underline{Q}}_{\Delta\theta} \underline{\underline{R}}_{\Delta\theta} \underline{\underline{K}}_{N} \underline{\underline{u}}_{N} \underline{\underline{u}}_{N}^T \underline{\underline{R}}_{\Delta\theta}^T \underline{\underline{P}}_{pq}^T \underline{\underline{T}}_{pq}^T \right)$$

$$+ \frac{1}{2R_f\delta} \sum_{p=1}^{m+1} \sum_{q=1}^{m+1} \text{Diag} \left(\underline{\underline{Q}}_{\Delta\theta} \underline{\underline{R}}_{\Delta\theta} \underline{\underline{K}}_{xy} \underline{\underline{u}}_{xy} \underline{\underline{u}}_{xy}^T \underline{\underline{R}}_{\Delta\theta}^T \underline{\underline{P}}_{pq}^T \underline{\underline{D}}_{pq}^T \underline{\underline{T}}_{pq}^T \right)$$

$$+ \frac{1}{2R_f\delta} \sum_{p=1}^{m+1} \sum_{q=1}^{m+1} \text{Diag} \left(\underline{\underline{Q}}_{\Delta\theta} \underline{\underline{R}}_{\Delta\theta} \underline{\underline{K}}_{N} \underline{\underline{u}}_{N} \underline{\underline{u}}_{N}^T \underline{\underline{R}}_{\Delta\theta}^T \underline{\underline{P}}_{pq}^T \underline{\underline{D}}_{pq}^T \underline{\underline{T}}_{pq}^T \right)$$

$$+ \frac{1}{2R_f\delta} \sum_{p=1}^{m+1} \sum_{q=1}^{m+1} \text{Diag} \left(\underline{\underline{DQ}}_{\Delta\theta} \underline{\underline{R}}_{\Delta\theta} \underline{\underline{K}}_{xy} \underline{\underline{u}}_{xy} \underline{\underline{u}}_{xy}^T \underline{\underline{R}}_{\Delta\theta}^T \underline{\underline{P}}_{pq}^T \underline{\underline{T}}_{pq}^T \right)$$

$$+ \frac{1}{2R_f\delta} \sum_{p=1}^{m+1} \sum_{q=1}^{m+1} \text{Diag} \left(\underline{\underline{DQ}}_{\Delta\theta} \underline{\underline{R}}_{\Delta\theta} \underline{\underline{K}}_{N} \underline{\underline{u}}_{N} \underline{\underline{u}}_{N}^T \underline{\underline{R}}_{\Delta\theta}^T \underline{\underline{P}}_{pq}^T \underline{\underline{T}}_{pq}^T \right)$$

$$\begin{aligned}
& + \frac{1}{2R_f\delta} \sum_{p=1}^{m+1} \sum_{q=1}^{m+1} \text{Diag} \left(\underline{\underline{Q}}_{\Delta\theta} \underline{\underline{R}}_{\Delta\theta} \underline{\underline{K}}_{\Delta\theta} \frac{\partial \underline{\underline{u}}_{xy}}{\partial \delta} \underline{\underline{u}}_{xy}^T \underline{\underline{R}}_{\Delta\theta}^T \underline{\underline{P}}_{\Delta\theta}^T \underline{\underline{T}}_{\Delta\theta}^T \right) \\
& + \frac{1}{2R_f\delta} \sum_{p=1}^{m+1} \sum_{q=1}^{m+1} \text{Diag} \left(\underline{\underline{Q}}_{\Delta\theta} \underline{\underline{R}}_{\Delta\theta} \underline{\underline{K}}_{\Delta\theta} \frac{\partial \underline{\underline{u}}_N}{\partial \delta} \underline{\underline{u}}_N^T \underline{\underline{R}}_{\Delta\theta}^T \underline{\underline{P}}_{\Delta\theta}^T \underline{\underline{T}}_{\Delta\theta}^T \right) \\
& + \frac{1}{2R_f\delta} \sum_{p=1}^{m+1} \sum_{q=1}^{m+1} \text{Diag} \left(\underline{\underline{Q}}_{\Delta\theta} \underline{\underline{R}}_{\Delta\theta} \underline{\underline{K}}_{\Delta\theta} \underline{\underline{u}}_{xy} \frac{\partial \underline{\underline{u}}_{xy}^T}{\partial \delta} \underline{\underline{R}}_{\Delta\theta}^T \underline{\underline{P}}_{\Delta\theta}^T \underline{\underline{T}}_{\Delta\theta}^T \right) \\
& + \frac{1}{2R_f\delta} \sum_{p=1}^{m+1} \sum_{q=1}^{m+1} \text{Diag} \left(\underline{\underline{Q}}_{\Delta\theta} \underline{\underline{R}}_{\Delta\theta} \underline{\underline{K}}_{\Delta\theta} \underline{\underline{u}}_N \frac{\partial \underline{\underline{u}}_N^T}{\partial \delta} \underline{\underline{R}}_{\Delta\theta}^T \underline{\underline{P}}_{\Delta\theta}^T \underline{\underline{T}}_{\Delta\theta}^T \right); \quad (19)
\end{aligned}$$

which, after refactoring, provides

$$\begin{aligned}
\frac{\partial \underline{\underline{G}}}{\partial \delta} &= \frac{1}{\delta} \underline{\underline{G}} + \frac{1}{2R_f\delta} \sum_{p=1}^{m+1} \sum_{q=1}^{m+1} \text{Diag} \\
&\times \left(\underline{\underline{Q}}_{\Delta\theta} \underline{\underline{R}}_{\Delta\theta} \left(\underline{\underline{K}}_{\Delta\theta} \underline{\underline{u}}_{xy} + \underline{\underline{K}}_{\Delta\theta} \underline{\underline{u}}_N \right) \underline{\underline{u}}_{xy}^T \underline{\underline{R}}_{\Delta\theta}^T \underline{\underline{P}}_{\Delta\theta}^T \underline{\underline{T}}_{\Delta\theta}^T \right) \\
&+ \frac{1}{2R_f\delta} \sum_{p=1}^{m+1} \sum_{q=1}^{m+1} \text{Diag} \\
&\times \left(\underline{\underline{DQ}}_{\Delta\theta} \underline{\underline{R}}_{\Delta\theta} \left(\underline{\underline{K}}_{\Delta\theta} \underline{\underline{u}}_{xy} + \underline{\underline{K}}_{\Delta\theta} \underline{\underline{u}}_N \right) \underline{\underline{u}}_{xy}^T \underline{\underline{R}}_{\Delta\theta}^T \underline{\underline{P}}_{\Delta\theta}^T \underline{\underline{T}}_{\Delta\theta}^T \right) \\
&+ \frac{1}{R_f\delta} \sum_{p=1}^{m+1} \sum_{q=1}^{m+1} \text{Diag} \left(\underline{\underline{Q}}_{\Delta\theta} \underline{\underline{R}}_{\Delta\theta} \underline{\underline{K}}_{\Delta\theta} \frac{\partial \underline{\underline{u}}_{xy}}{\partial \delta} \underline{\underline{u}}_{xy}^T \underline{\underline{R}}_{\Delta\theta}^T \underline{\underline{P}}_{\Delta\theta}^T \underline{\underline{T}}_{\Delta\theta}^T \right) \\
&+ \frac{1}{2R_f\delta} \sum_{p=1}^{m+1} \sum_{q=1}^{m+1} \text{Diag} \left(\underline{\underline{Q}}_{\Delta\theta} \underline{\underline{R}}_{\Delta\theta} \underline{\underline{K}}_{\Delta\theta} \frac{\partial \underline{\underline{u}}_N}{\partial \delta} \underline{\underline{u}}_N^T \underline{\underline{R}}_{\Delta\theta}^T \underline{\underline{P}}_{\Delta\theta}^T \underline{\underline{T}}_{\Delta\theta}^T \right)
\end{aligned}$$

$$+ \frac{1}{2R_f\delta} \sum_{p=1}^{m+1} \sum_{q=1}^{m+1} \text{Diag} \left(\underline{\underline{Q}}_{\Delta\theta} \underline{\underline{R}}_{\Delta\theta} \underline{\underline{K}}_{\Delta\theta} \underline{\underline{u}}_N \frac{\partial \underline{\underline{u}}_{xy}^T}{\partial \delta} \underline{\underline{R}}_{\Delta\theta}^T \underline{\underline{P}}_{\Delta\theta}^T \underline{\underline{T}}_{\Delta\theta}^T \right). \quad (20)$$

Following the asymptotic analysis of [1,3], in the case of an *open crack* the displacement in the crack tip neighborhood will have a functional form of the type

$$u(\delta) \sim \sqrt{\delta} (\sin, \cos) (\epsilon \log \delta) \quad \text{with} \quad \epsilon = \frac{1}{2\pi} \log \left(\frac{1-\beta}{1+\beta} \right) \quad (21)$$

and β is Dundurs' parameter introduced in Section 1. Application of Equation (21) to the terms on the right hand side of Eq. (20) provides:

$$\underline{\underline{u}}_{xy}, \underline{\underline{u}}_N \sim u(\delta) \sim \sqrt{\delta} (\sin, \cos) (\epsilon \log \delta) \xrightarrow{\delta \rightarrow 0} 0; \quad (22)$$

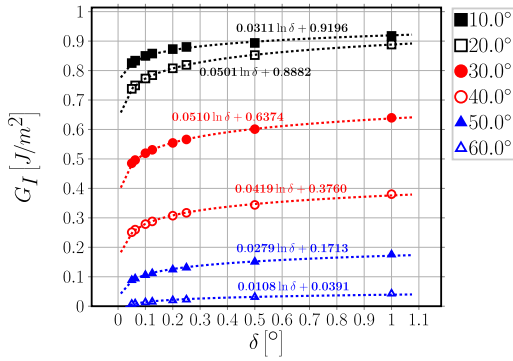
$$\underline{\underline{u}}_{xy} \underline{\underline{u}}_{xy}^T, \underline{\underline{u}}_N \underline{\underline{u}}_N^T \sim u^2(\delta) \sim \delta (\sin^2, \cos^2, \sin \cdot \cos) (\epsilon \log \delta) \xrightarrow{\delta \rightarrow 0} 0; \quad (23)$$

$$\begin{aligned}
\frac{\partial \underline{\underline{u}}_{xy}}{\partial \delta} \underline{\underline{u}}_{xy}^T, \frac{\partial \underline{\underline{u}}_N}{\partial \delta} \underline{\underline{u}}_N^T &\sim -\frac{1}{2} (\sin^2, \cos^2, \sin \cdot \cos) (\epsilon \log \delta) \\
&+ (-\sin^2, \cos^2, \pm \sin \cdot \cos) (\epsilon \log \delta) \xrightarrow{\delta \rightarrow 0} \text{finite}; \quad (24)
\end{aligned}$$

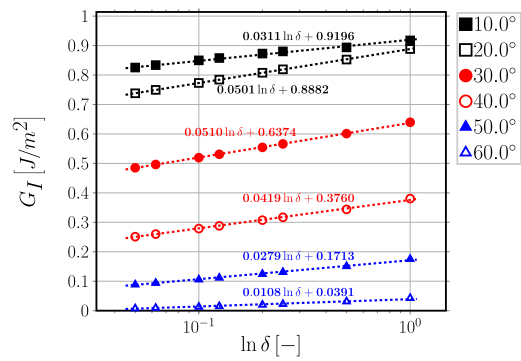
$$\underline{\underline{G}} \sim \frac{1}{\delta} \underline{\underline{u}}_{xy} \underline{\underline{u}}_{xy}^T \sim \frac{1}{\delta} u^2(\delta) \sim (\sin^2, \cos^2, \sin \cdot \cos) (\epsilon \log \delta) \xrightarrow{\delta \rightarrow 0} \text{finite}. \quad (25)$$

In Equations (22)–(25), the multiplication by a trigonometric function of the type $(\sin, \cos, \sin^2, \cos^2, \sin \cdot \cos)$ prevents the divergence of the asymptote. Recalling Eqs. (5) and (6), in the limit of $\delta \rightarrow 0$ the rotation matrices become equal to the identity matrix:

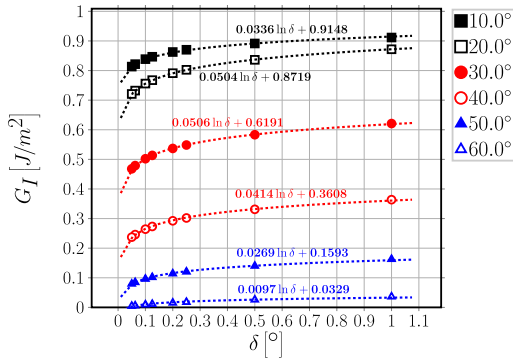
$$\underline{\underline{P}}_{\Delta\theta}, \underline{\underline{Q}}_{\Delta\theta} \xrightarrow{\delta \rightarrow 0} \begin{bmatrix} 1 & 0 \\ 0 & 1 \end{bmatrix}. \quad (26)$$



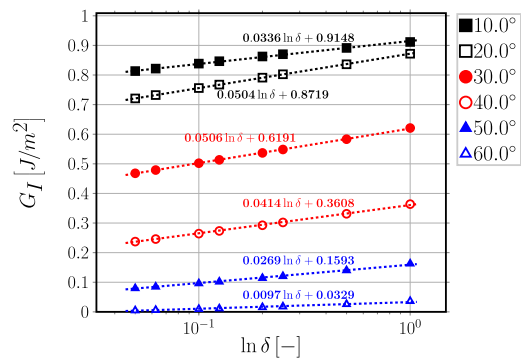
(a) 1st order elements.



(b) 1st order elements.



(c) 2nd order elements.



(d) 2nd order elements.

Fig. 8. Logarithmic dependence on δ of Mode I ERR: interpolation of numerical results for $V_f = 40\%$.

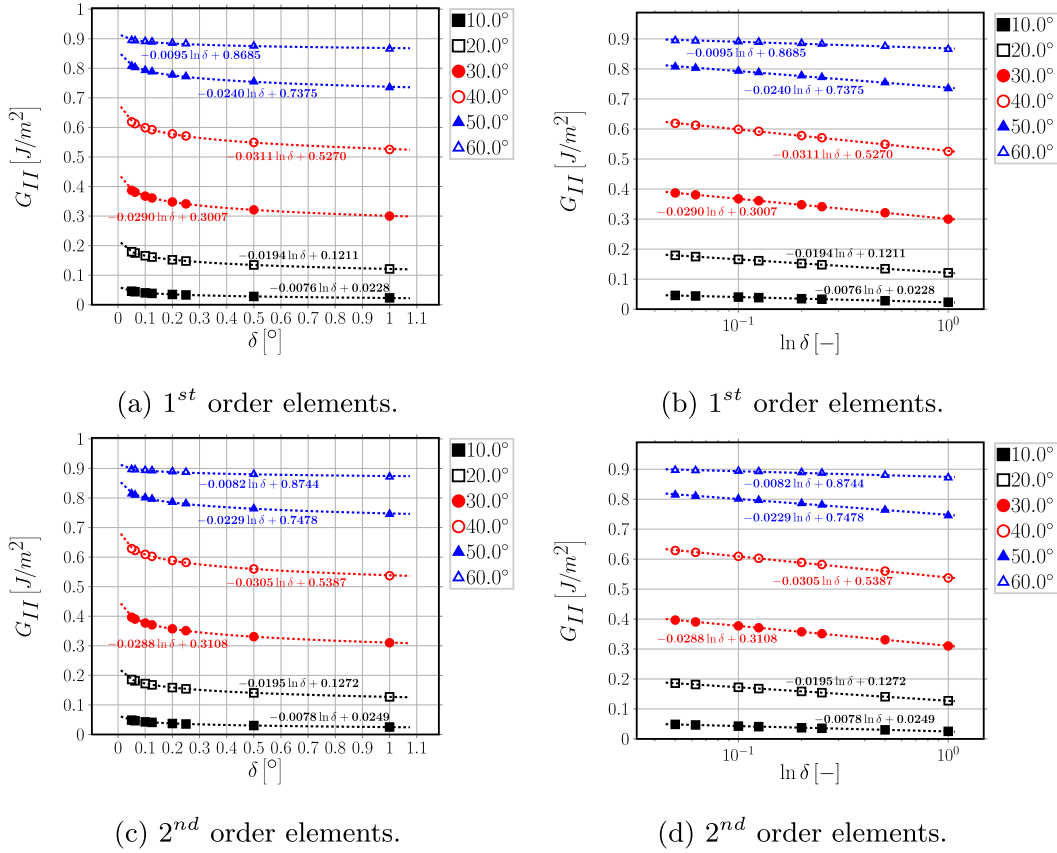


Fig. 9. Logarithmic dependence on δ of Mode II ERR: interpolation of numerical results for $V_f = 0.1\%$.

Applying the results of Equations (22)–(26) to Eq. (20), it can be shown that the derivative of \underline{G} can be split in a factor that goes to 0 in the limit of $\delta \rightarrow 0$ and in a factor independent of δ :

$$\lim_{\delta \rightarrow 0} \frac{\partial \underline{G}}{\partial \delta} \sim \frac{1}{\delta} \left(\underline{E}(\delta)^0 + \underline{C} \right). \quad (27)$$

Thus, asymptotically, the Mode I and Mode II Energy Release Rate behave like the logarithm of the angular size δ of the elements in the crack tip neighborhood:

$$\lim_{\delta \rightarrow 0} \frac{\partial \underline{G}}{\partial \delta} \sim \frac{1}{\delta} \xrightarrow{f \delta} \lim_{\delta \rightarrow 0} \underline{G} \sim \underline{A} \log(\delta) + \underline{B}. \quad (28)$$

5.2. Numerical results

Evaluations of the Mode I, Mode II and total Energy Release Rate using the VCCT applied to the FE solution of the fiber-matrix interface crack in the single fiber model of Sec. 2 are reported respectively in Figs. 4–6.

Results for Mode I ERR in Fig. 4 show clearly the transition from the *open* crack regime, where Mode I ERR is different from zero, to the *closed* crack regime of the debond, where $G_I = 0$. Looking at Fig. 4, the crack is *open* for $\Delta\theta \leq 60^\circ$ and it is *closed*, i.e. a contact zone is present, for $\Delta\theta \geq 70^\circ$. As expected from the analysis of the previous section, and given that Mode I ERR is different from zero only in the *open* crack regime, a significant dependence on the element size δ can be observed in Fig. 4 when using both 1st and 2nd order elements and with both an effectively infinite ($V_f = 0.1\%$) and finite size ($V_f = 40\%$) matrix. At first sight, it is immediate to see from Fig. 4 that a decrease in δ leads to a decrease in G_I . However, two further effects can be observed due to the refinement of the mesh at the crack tip, i.e. the decrease of the element size δ . First, the occurrence of the peak G_I is shifted to

lower angles for very low volume fractions: it occurs at $\Delta\theta = 30^\circ$ with $\delta = 1.0^\circ, 0.5^\circ$ and at $\Delta\theta = 20^\circ$ with $\delta \leq 0.25^\circ$ for both 1st and 2nd order elements and $V_f = 0.1\%$. Second, the appearance of the contact zone, i.e. the switch to the *closed* crack regime, is anticipated to smaller debonds: it occurs at $\Delta\theta = 70^\circ$ with $\delta \geq 0.2^\circ$ and at $\Delta\theta = 60^\circ$ with $\delta < 0.2^\circ$ for both 1st and 2nd order elements and both $V_f = 0.1\%$ and $V_f = 40\%$.

Observing Fig. 5, it is possible to notice the existence of two distinct regimes in the behavior of G_{II} with respect to the element size δ . For $\Delta\theta \leq 60^\circ$, G_{II} depends on the value of δ , while $\Delta\theta \geq 70^\circ$ it is effectively independent of the element size at the crack tip for both 1st and 2nd order elements and both an effectively infinite ($V_f = 0.1\%$) and finite size ($V_f = 40\%$) matrix. Comparing the value of $\Delta\theta$ at which the change from the δ -dependency regime to the δ -independency regime occurs for G_{II} with Mode I ERR in Fig. 4, it is possible to observe that the δ -dependency regime change of Mode II ERR coincides with the onset of the contact zone, i.e. the transition from *open* crack regime to the *closed* crack regime. The result confirms the analytical considerations of the previous section: for an *open* crack both Mode I and Mode II ERR depend on the element size δ at the crack tip.

Further observation of Fig. 5 reveals that, in the *open* crack regime, decreasing the element size δ causes an increase of Mode II ERR. Similarly to Mode I ERR, a shift of the peak G_{II} can also be observed for $V_f = 0.1\%$: the maximum value of G_{II} occurs at $\Delta\theta = 70^\circ$ for $\delta > 0.25^\circ$ for 1st order elements and for $\delta > 0.5^\circ$ for 2nd order elements, while it is shifted to $\Delta\theta = 60^\circ$ for $\delta \leq 0.25^\circ$ for 1st order elements and for $\delta \leq 0.5^\circ$ for 2nd order elements.

Analysis of the total ERR in Fig. 6 leads to an observation that was not predicted by the considerations of the previous section: G_{TOT} is effectively independent of the element size δ in both the *open* and the *closed* crack regimes, at least for reasonably small elements ($\delta \leq 1.0^\circ$). Given that $G_{II} = G_{TOT}$ for the *closed* crack, it explains the independency of G_{II} from δ after the onset of the contact zone.

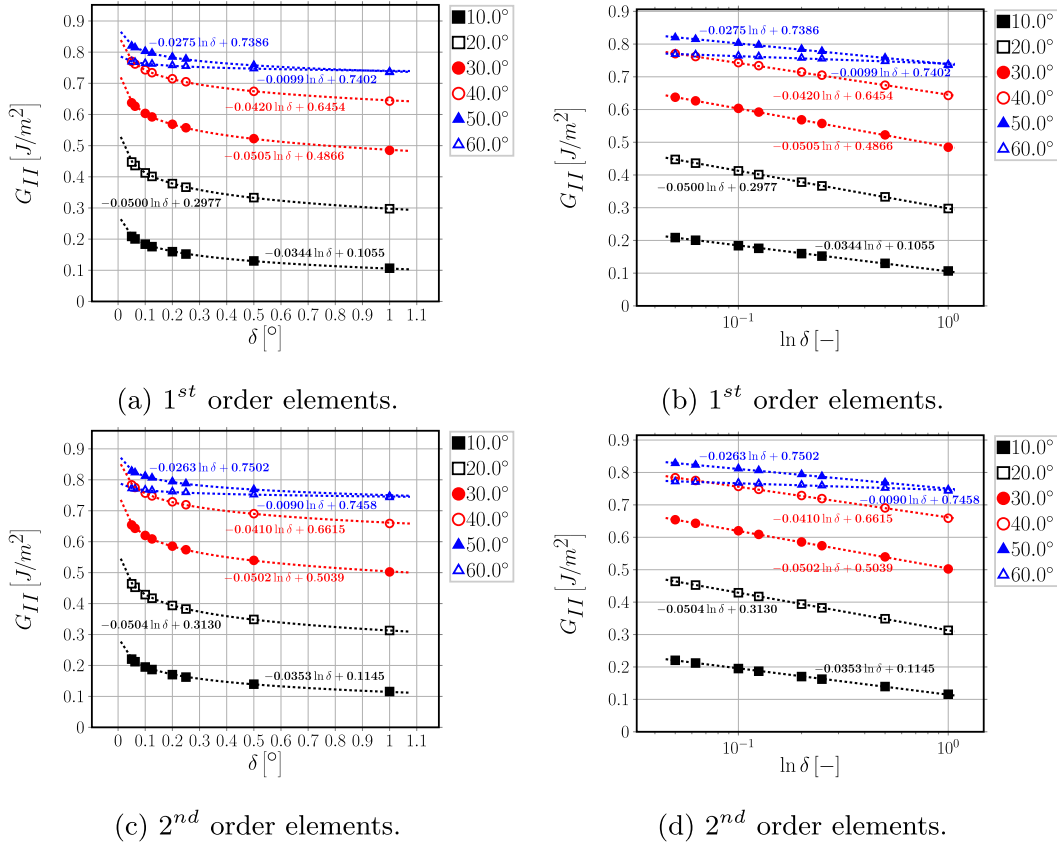


Fig. 10. Logarithmic dependence on δ of Mode II ERR: interpolation of numerical results for $V_f = 40\%$.

Table 2

Summary of linear regression results and main statistical tests for Mode I ERR.

$V_{f[\%]}$	Order	$\Delta\theta [^\circ]$	$A \left[\frac{J}{m^2} \right]$	$B \left[\frac{J}{m^2} \right]$	$r [-]$	$r^2 [-]$	$p(A) [-]$	$p(B) [-]$
0.1	1	10.0	0.0064	0.2113	0.9933	0.9866	7.48E-07	3.49E-14
		20.0	0.0183	0.3331	0.9996	0.9992	1.44E-10	2.40E-16
		30.0	0.0280	0.3392	1.0000	1.0000	2.25E-16	4.26E-21
		40.0	0.0304	0.2524	0.9997	0.9995	4.38E-11	7.94E-15
		50.0	0.0235	0.1278	0.9985	0.9970	8.61E-09	2.01E-11
		60.0	0.0094	0.0284	0.9854	0.9709	7.75E-06	6.14E-07
0.1	2	10.0	0.0069	0.2103	0.9962	0.9924	1.36E-07	1.03E-14
		20.0	0.0187	0.3277	0.9997	0.9994	7.85E-11	1.62E-16
		30.0	0.0280	0.3296	1.0000	1.0000	3.28E-16	7.29E-21
		40.0	0.0298	0.2408	0.9997	0.9995	4.82E-11	1.04E-14
		50.0	0.0225	0.1177	0.9984	0.9967	1.10E-08	3.27E-11
		60.0	0.0081	0.0228	0.9811	0.9626	1.66E-05	2.17E-06
40	1	10.0	0.0311	0.9196	0.9963	0.9927	1.03E-07	9.33E-15
		20.0	0.0501	0.8882	1.0000	0.9999	1.21E-13	2.33E-19
		30.0	0.0510	0.6374	0.9998	0.9996	1.66E-11	2.58E-16
		40.0	0.0419	0.3760	0.9988	0.9976	4.56E-09	5.25E-13
		50.0	0.0279	0.1713	0.9980	0.9961	2.22E-08	2.52E-11
		60.0	0.0108	0.0391	0.9901	0.9804	3.44E-06	9.46E-08
40	2	10.0	0.0336	0.9148	0.9988	0.9977	3.45E-09	5.09E-16
		20.0	0.0504	0.8719	1.0000	1.0000	3.70E-14	8.26E-20
		30.0	0.0506	0.6191	0.9999	0.9997	7.63E-12	1.35E-16
		40.0	0.0414	0.3608	0.9994	0.9989	4.95E-10	6.80E-14
		50.0	0.0269	0.1593	0.9982	0.9964	1.66E-08	2.31E-11
		60.0	0.0097	0.0329	0.9890	0.9781	4.96E-06	1.99E-07

Analysis of Figs. 4–6 has shown the dependency of Mode I and Mode II ERR on the element size δ . Following the derivations of the previous section, we model the dependency of G_I and G_{II} with respect to δ as

$$G_{(I)} = A(\Delta\theta) \ln \delta + B(\Delta\theta), \quad (29)$$

where $A(\Delta\theta)$ and $B(\Delta\theta)$ are parameters dependent on $\Delta\theta$ estimated through linear regression (with $x = \ln \delta$) of the numerical results.

As shown in Figs. 7–10 both in linear and logarithmic scales of δ , the result is remarkable: both the correlation coefficient r and the r^2 ratio (of explained to total variance) are always greater than 0.95 and the p -values of the coefficients A and B are at least $< 1E - 6$ and often $< 1E - 11$ (see Table 2 for G_I and Table 3 for G_{II}). The results of the linear regression confirm the analytical derivations of the previous section, which showed the logarithmic behavior of Mode I and

Table 3
Summary of linear regression results and main statistical tests for Mode II ERR.

$V_{[\%]}$	Order	$\Delta\theta [^\circ]$	$A \left[\frac{J}{m} \right]$	$B \left[\frac{J}{m} \right]$	$r [-]$	$r^{2[-]}$	$p(A) [-]$	$p(B) [-]$
0.1	1.0	10.0	-0.0076	0.0228	-0.9996	0.9991	2.09E-10	1.64E-11
		20.0	-0.0194	0.1211	-1.0000	1.0000	1.99E-15	2.02E-18
		30.0	-0.0290	0.3007	-0.9999	0.9998	4.12E-12	1.97E-16
		40.0	-0.0311	0.5270	-0.9995	0.9989	4.13E-10	1.05E-15
		50.0	-0.0240	0.7375	-0.9979	0.9958	2.32E-08	1.66E-15
		60.0	-0.0095	0.8685	-0.9835	0.9672	1.12E-05	1.22E-15
0.1	2.0	10.0	-0.0078	0.0249	-0.9996	0.9992	1.91E-10	1.06E-11
		20.0	-0.0196	0.1272	-1.0000	1.0000	3.48E-15	2.78E-18
		30.0	-0.0288	0.3108	-0.9999	0.9998	1.45E-12	5.47E-17
		40.0	-0.0305	0.5387	-0.9995	0.9990	3.32E-10	6.55E-16
		50.0	-0.0229	0.7478	-0.9979	0.9959	2.17E-08	1.09E-15
		60.0	-0.0082	0.8744	-0.9806	0.9615	1.81E-05	8.26E-16
40.0	1.0	10.0	-0.0344	0.1055	-0.9997	0.9995	3.82E-11	2.73E-12
		20.0	-0.0500	0.2977	-1.0000	0.9999	4.22E-14	5.66E-17
		30.0	-0.0505	0.4866	-0.9999	0.9997	6.44E-12	4.82E-16
		40.0	-0.0420	0.6454	-0.9996	0.9991	2.12E-10	9.66E-16
		50.0	-0.0275	0.7386	-0.9985	0.9971	9.01E-09	1.44E-15
		60.0	-0.0099	0.7402	-0.9926	0.9853	1.41E-06	5.13E-16
40.0	2.0	10.0	-0.0353	0.1145	-0.9998	0.9995	2.92E-11	1.50E-12
		20.0	-0.0504	0.3130	-1.0000	0.9999	4.00E-14	4.17E-17
		30.0	-0.0502	0.5039	-0.9999	0.9998	2.87E-12	1.69E-16
		40.0	-0.0410	0.6615	-0.9996	0.9992	2.02E-10	6.89E-16
		50.0	-0.0263	0.7502	-0.9987	0.9973	6.87E-09	7.76E-16
		60.0	-0.0090	0.7458	-0.9921	0.9842	1.79E-06	3.37E-16

Mode II ERR. Similar conclusions were reached in Refs. [29,31] for a straight bi-material crack with respect to the parameter $\Delta a/a$; however, no functional expression of $G_{(c)}$ was proposed.

6. Conclusions & outlook

The application of the Virtual Crack Closure Technique to the calculation of Mode I, Mode II and total Energy Release Rate was analyzed in the context of the Finite Element solution of the bi-material circular arc crack, or fiber-matrix interface crack. A synthetic vectorial formulation of the VCCT has been proposed and its usefulness exemplified in the analysis of the mesh dependency. By both analytical considerations and numerical simulations, it has been shown that:

- the total ERR is invariant to rotations of the reference frame (and more in general to linear transformations), which implies that rotation of crack tip forces and displacement is actually not required in the use of the VCCT for the calculation of G_{TOT} ;
- the total ERR does not depend on the size δ of the elements at the crack tip, at least for reasonably small elements ($\delta \leq 1.0^\circ$);
- as a consequence, Mode II ERR for the *closed* interface crack does not depend on δ , as $G_{II} = G_{TOT}$ after the onset of the contact zone;
- for the *open* interface crack, Mode I and Mode II ERR depend on the element size δ through a logarithmic law of the type $A(\Delta\theta) \ln \delta + B(\Delta\theta)$;
- the sign of the logarithm is always positive for G_I , i.e. it decreases when δ decreases, and negative for G_{II} , i.e. it increases when δ decreases.

The conclusion is significant: as the behavior of Mode I and Mode II is logarithmic with respect to mesh size, there exists no asymptotic limit and thus no convergence of the values. A convergence analysis based on the reduction of the error between successive iterations would not provide a reliable assessment of the accuracy of the FE solution of Mode I and Mode II Energy Release Rate of the fiber-matrix interface crack. A validation is thus required with respect to data obtained through a different method, be it analytical, numerical or experimen-

tal. Moreover, it has been shown that: first, the same behavior appears when using 1st as well as 2nd order elements; second, no improvement is expected with the use of singular elements, as the logarithmic dependency of G_I and G_{II} is governed by the definition of ERR itself together with the asymptotic behavior of the displacement field at the crack tip. These two conclusions put into discussion recommendations often provided by manuals of commercial FEM packages such as Abaqus [36]. The latter for example, in the context of VCCT-based crack propagation (Section 11.4.2 of the *Abaqus Analysis User's Guide*), suggests that *in most cases mesh refinement will help with obtaining a realistic result, that results with nonlinear materials are more sensitive to meshing than results with small-strain linear elasticity* and that *first-order elements generally work best for crack propagation analysis*. The previous considerations might apply for cracks in isotropic mediums; however, the VCCT-based crack propagation technique is proposed in Abaqus as a suitable technique for surface-based simulation of bi-material interface debonding. We have shown that, for a circular interface crack: mesh-refinement (*h-refinement*) does not guarantee convergence of Mode I and Mode II ERR, as their dependency on element size is logarithmic; sensitivity to meshing is actually very significant in small-strain linear elasticity and depends on the nature of the linear elastic solution at the crack tip; no difference in convergence trends is observable between first and second order elements (*p-refinement*). This closing considerations are not meant to be a critique *per se* to commercial software, but rather as a source of reflection on the best use of software tools. Apart from the scientific merit of the results proposed, the conclusions presented here stand as an invitation to the practitioner to avoid black-box thinking and blind application of built-in software solutions.

Declaration of competing interest

No conflict of interests exists.

Acknowledgements

Luca Di Stasio thanks Prof. Janis Varna for the useful discussions and suggestions. Luca Di Stasio gratefully acknowledges the support of the European School of Materials (EUSMAT) through the DocMASE Doctoral Programme and the European Commission through the Erasmus Mundus Programme.

Appendix A. Derivation of the relationship between crack tip forces and displacements for first order quadrilateral elements

Appendix A.1. Foundational relations

We review and present in this Section the foundational relations of the isoparametric formulation of the Finite Element Method. The objective here is to provide a theoretical foundation to the expressions in Equation (10) and Equation (11) and a reference for the explicit calculation of the nodal stiffness matrices proposed in Eq. (10) and Eq. (11). We propose a general treatment, valid for 2- and 3-dimensional problems, so that the interested reader could evaluate the nodal stiffness matrices for both a 2- and a 3-dimensional crack. However, in order to clarify the structure of some specific objects, we explicitly write their 2-dimensional form, which is of interest for the problem of this paper.

Denoting by d the number of geometrical dimensions of the problem ($d = 2$ in the present work), the element Jacobian J and its inverse J^{-1} can be expressed in general as

$$J_{ij} = (e_{\xi_j})_i = \frac{\partial x_i}{\partial \xi_j} \quad J_{ij}^{-1} = (e^{x_j})_i = \frac{\partial \xi_i}{\partial x_j} \quad i, j = 1, \dots, d \quad (\text{A.1})$$

where (e_{ξ_j}) and (e^{x_j}) are respectively the covariant and contravariant basis vectors of the mapping between global $\{x_i\}$ and local element $\{\xi_i\}$ coordinates.

In 2D, assuming the global coordinates are $\{x, y\}$ and the local element coordinates are $\{\xi, \eta\}$, the covariant and contravariant basis vectors assume the form

$$\underline{e}_{\xi} = \begin{bmatrix} \frac{\partial x}{\partial \xi} \\ \frac{\partial y}{\partial \xi} \end{bmatrix} \quad \underline{e}_{\eta} = \begin{bmatrix} \frac{\partial x}{\partial \eta} \\ \frac{\partial y}{\partial \eta} \end{bmatrix}, \quad (\text{A.2})$$

$$\underline{e}_x = \begin{bmatrix} \frac{\partial \xi}{\partial x} \\ \frac{\partial \eta}{\partial x} \end{bmatrix} \quad \underline{e}_y = \begin{bmatrix} \frac{\partial \xi}{\partial y} \\ \frac{\partial \eta}{\partial y} \end{bmatrix}. \quad (\text{A.3})$$

and the element Jacobian J and its inverse J^{-1} can be computed for a 2D problem as

$$\underline{\underline{J}} = [\underline{e}_{\xi} | \underline{e}_{\eta}] = \begin{bmatrix} \frac{\partial x}{\partial \xi} & \frac{\partial x}{\partial \eta} \\ \frac{\partial y}{\partial \xi} & \frac{\partial y}{\partial \eta} \end{bmatrix} \quad \underline{\underline{J}}^{-1} = [\underline{e}^x | \underline{e}^y] = \begin{bmatrix} \frac{\partial \xi}{\partial x} & \frac{\partial \xi}{\partial y} \\ \frac{\partial \eta}{\partial x} & \frac{\partial \eta}{\partial y} \end{bmatrix}. \quad (\text{A.4})$$

Denoting by \underline{p} the $d \times 1$ position vector in global coordinates, we can formally introduce the $3(d-1) \times d$ matrix operator of partial differentiation $\underline{\underline{B}}$ such that

$$\underline{\underline{\varepsilon}}(\underline{p}) = \underline{\underline{B}} \cdot \underline{u}(\underline{p}), \quad (\text{A.5})$$

where \underline{u} and $\underline{\underline{\varepsilon}}$ are respectively the $d \times 1$ displacement vector and the $3(d-1) \times 1$ strain vector in Voigt notation. Denoting by n the number of nodes of a generic element, it holds that $n = s \times m$ where s represents the number of sides of the element (3 for a triangle, 4 for a rectangle, ...) and m the order of the shape functions (1 for linear shape functions, 2 for quadratic shape functions, ...). We can now introduce the $d \times d \cdot n$ matrix $\underline{\underline{N}}$ of shape functions such that

$$\underline{u} = \underline{\underline{N}} \cdot \underline{u}_N, \quad (\text{A.6})$$

where \underline{u}_N is the $d \cdot n \times 1$ vector of element nodal variables. Having introduced $\underline{\underline{B}}$ and $\underline{\underline{N}}$ in Equations (A.5) and (A.6) respectively, it is possible to define the $3(d-1) \times d \cdot n$ matrix $\underline{\underline{B}}$ of derivatives (with respect to global coordinates) of shape functions as

$$\underline{\underline{B}} = \underline{\underline{B}} \cdot \underline{\underline{N}}. \quad (\text{A.7})$$

We introduce the linear elastic material behavior in the form of the $3(d-1) \times 3(d-1)$ rigidity matrix $\underline{\underline{D}}$ such that

$$\underline{\underline{\sigma}} = \underline{\underline{D}} \cdot \underline{\underline{\varepsilon}}, \quad (\text{A.8})$$

where $\underline{\underline{\sigma}}$ the $3(d-1) \times 1$ stress vector in Voigt notation. It is finally possible to define the $n \times n$ element stiffness matrix $\underline{\underline{k}}_e$ as

$$\underline{\underline{k}}_e = \int_{V_e(x_i)} (\underline{\underline{B}}^T \underline{\underline{D}} \cdot \underline{\underline{B}}) dV_e(x_i) = \int_{V_e(\xi_i)} (\underline{\underline{B}}^T \underline{\underline{D}} \cdot \underline{\underline{B}}) \sqrt{g} dV_e(\xi_i), \quad (\text{A.9})$$

where $g = \det(\underline{\underline{J}}^T \underline{\underline{J}})$ and V_e is the element volume. Given that isoparametric elements are always defined between -1 and 1 in each dimension, Equation (A.9) can be simplified to

$$\underline{\underline{k}}_e = \int_{-1}^1 \dots \int_{-1}^1 (\underline{\underline{B}}^T \underline{\underline{D}} \cdot \underline{\underline{B}}) \sqrt{g} d\xi_i, \quad (\text{A.10})$$

which is amenable to numerical integration by means of a Gaussian quadrature of the form

$$\underline{\underline{k}}_e \approx \underbrace{\sum_{k=1}^N \dots \sum_{h=1}^N}_{d \text{ times}} w_k \dots w_h \left(\underline{\underline{B}}^T(\xi_i(k, \dots, h)) \cdot \underline{\underline{D}} \cdot \underline{\underline{B}}(\xi_i(k, \dots, h)) \sqrt{g} \right), \quad (\text{A.11})$$

where $\xi_i(k, \dots, h)$ are the coordinates of the N Gaussian quadrature points. The element stiffness matrix as evaluated in Eq. (A.11) is in general a full symmetric matrix in the case of linear elasticity. For 2D rectangular elements with quadratic shape functions (8-nodes serendipity elements), the element stiffness matrix has the form

$$\underline{\underline{k}}_e = \begin{bmatrix} k_{e|11} & k_{e|12} & k_{e|13} & k_{e|14} & k_{e|15} & k_{e|16} & k_{e|17} & k_{e|18} \\ k_{e|12} & k_{e|22} & k_{e|23} & k_{e|24} & k_{e|25} & k_{e|26} & k_{e|27} & k_{e|28} \\ k_{e|13} & k_{e|23} & k_{e|33} & k_{e|34} & k_{e|35} & k_{e|36} & k_{e|37} & k_{e|38} \\ k_{e|14} & k_{e|24} & k_{e|34} & k_{e|44} & k_{e|45} & k_{e|46} & k_{e|47} & k_{e|48} \\ k_{e|15} & k_{e|25} & k_{e|35} & k_{e|45} & k_{e|55} & k_{e|56} & k_{e|57} & k_{e|58} \\ k_{e|16} & k_{e|26} & k_{e|36} & k_{e|46} & k_{e|56} & k_{e|66} & k_{e|67} & k_{e|68} \\ k_{e|17} & k_{e|27} & k_{e|37} & k_{e|47} & k_{e|57} & k_{e|67} & k_{e|77} & k_{e|78} \\ k_{e|18} & k_{e|28} & k_{e|38} & k_{e|48} & k_{e|58} & k_{e|68} & k_{e|78} & k_{e|88} \end{bmatrix}. \quad (\text{A.12})$$

Appendix A.2. Calculation of displacements and reaction forces

With reference to Fig. A.11, we define:

$u_{x,M}, u_{x,F}$ the x -displacement of the nodes belonging to the free side of the first element belonging to the crack, respectively on the matrix (bulk) and fiber (inclusion) side;

$u_{y,M}, u_{y,F}$ the y -displacement of the nodes belonging to the free side of the first element belonging to the crack, respectively on the matrix (bulk) and fiber (inclusion) side;

$u_{r,M}, u_{r,F}$ the r -displacement of the nodes belonging to the free side of the first element belonging to the crack, respectively on the matrix (bulk) and fiber (inclusion) side;

$u_{\theta,M}, u_{\theta,F}$ the θ -displacement of the nodes belonging to the free side of the first element belonging to the crack, respectively on the matrix (bulk) and fiber (inclusion) side;

$F_{x,CT}, F_{y,CT}$ respectively the x - and y -component of the reaction force at the crack tip;

$F_{r,CT}, F_{\theta,CT}$ respectively the r - and θ -component of the reaction force at the crack tip.

The $x - y$ reference frame is the global reference frame, while the $r - \theta$ reference frame is such that the θ direction coincides with the crack propagation direction at the crack tip and r the in-plane normal to the propagation direction. For an arc-crack as the present one, the r -direction coincides with the radial direction of the inclusion.

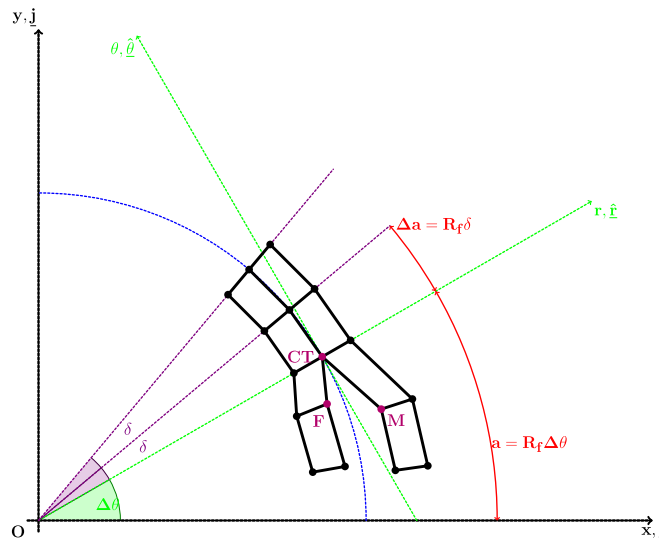


Fig. A.11 Schematic representation of the discretized crack tip geometry for 1st order quadrilateral elements.

The crack opening displacement u_r and the crack shear displacement u_θ at the crack tip can thus be written as

$$u_r = \cos(\Delta\theta) u_x + \sin(\Delta\theta) u_y \quad u_\theta = -\sin(\Delta\theta) u_x + \cos(\Delta\theta) u_y, \quad (\text{A.13})$$

where u_x and u_y are defined as

$$u_x = u_{x,M} - u_{x,F} \quad u_y = u_{y,M} - u_{y,F} \quad (\text{A.14})$$

and $2\Delta\theta$ is total angular size of the debond. The corresponding forces at the crack tip are

$$F_r = \cos(\Delta\theta)F_{x,CT} + \sin(\Delta\theta)F_{y,CT} \quad F_\theta = -\sin(\Delta\theta)F_{x,CT} + \cos(\Delta\theta)F_{y,CT}. \quad (\text{A.15})$$

At the crack tip, the FE mesh possesses two coincident points, labeled *FCT* and *MCT*. Continuity of the displacements at the crack tip must be ensured. Furthermore, in order to measure the force at the crack tip, a fully-constraint dummy node needs to be created and formally linked to the two nodes at the crack tip by the conditions

$$\begin{cases} u_{x,FCT} - u_{x,MCT} - u_{x,DUMMY} = 0 \\ u_{y,FCT} - u_{y,MCT} - u_{y,DUMMY} = 0 \\ u_{x,DUMMY} = 0 \\ u_{y,DUMMY} = 0 \end{cases}, \quad (\text{A.16})$$

which can be simplified to

$$\begin{cases} u_{x,FCT} = u_{x,MCT} \\ u_{y,FCT} = u_{y,MCT} \\ R_{x,DUMMY} = R_{x,FCT} = -R_{x,MCT} = F_{x,CT} \\ R_{y,DUMMY} = R_{y,FCT} = -R_{y,MCT} = F_{y,CT} \end{cases}. \quad (\text{A.17})$$

Making use of Eq. (A.12), four equations can be written in the four displacement $u_{x,FCT}$, $u_{x,MCT}$, $u_{y,FCT}$ and $u_{y,MCT}$:

$$\begin{cases} (k_{e,M|11} + k_{e,M|33})u_{x,MCT} + (k_{e,M|12} + k_{e,M|34})u_{y,MCT} \\ + k_{e,M|13}u_{x,M} + k_{e,M|14}u_{y,M} + (k_{M|17} + k_{M|35})u_{N,MC|7} + (k_{M|18} + k_{M|36})u_{N,MC|8} \\ + \sum_{i=5}^6 k_{M|1i}u_{N,MC|i} + \sum_{i=7}^8 k_{M|3i}u_{N,MB|i} + k_{M|31}u_{x,NCOI} + k_{M|32}u_{y,NCOI} = 0 \\ (k_{e,M|21} + k_{e,M|43})u_{x,MCT} + (k_{e,M|22} + k_{e,M|44})u_{y,MCT} \\ + k_{e,M|23}u_{x,M} + k_{e,M|24}u_{y,M} + (k_{M|27} + k_{M|45})u_{N,MC|7} + (k_{M|28} + k_{M|46})u_{N,MC|8} \\ + \sum_{i=5}^6 k_{M|2i}u_{N,MC|i} + \sum_{i=7}^8 k_{M|4i}u_{N,MB|i} + k_{M|41}u_{x,NCOI} + k_{M|42}u_{y,NCOI} = 0 \\ (k_{e,F|77} + k_{e,F|55})u_{x,FCT} + (k_{e,F|78} + k_{e,F|56})u_{y,FCT} \\ + k_{e,F|75}u_{x,F} + k_{e,F|76}u_{y,F} + (k_{F|71} + k_{F|53})u_{N,FC|1} + (k_{F|72} + k_{F|54})u_{N,FC|2} \\ + \sum_{i=2}^3 k_{F|7i}u_{N,FC|i} + \sum_{i=1}^2 k_{F|5i}u_{N,FB|i} + k_{F|57}u_{x,NCOI} + k_{F|58}u_{y,NCOI} = 0 \\ (k_{e,F|87} + k_{e,F|65})u_{x,FCT} + (k_{e,F|88} + k_{e,F|66})u_{y,FCT} \\ + k_{e,F|85}u_{x,F} + k_{e,F|86}u_{y,F} + (k_{F|81} + k_{F|63})u_{N,FC|1} + (k_{F|82} + k_{F|64})u_{N,FC|2} \\ + \sum_{i=2}^3 k_{F|8i}u_{N,FC|i} + \sum_{i=1}^2 k_{F|6i}u_{N,FB|i} + k_{F|67}u_{x,NCOI} + k_{F|68}u_{y,NCOI} = 0 \end{cases}. \quad (\text{A.18})$$

Solving for $u_{y,FCT}$ and $u_{y,MCT}$ the third and fourth relations in Eq. (A.18) and substituting in the first two expressions of Eq. (A.18), we get

$$\begin{cases} (k_{e,M|11} + k_{e,M|33} + k_{e,F|77} + k_{e,F|55})u_{x,MCT} + (k_{e,M|12} + k_{e,M|34} + k_{e,F|78} + k_{e,F|56})u_{y,MCT} + \\ + k_{e,M|13}u_{x,M} + k_{e,M|14}u_{y,M} + k_{e,F|75}u_{x,F} + k_{e,F|76}u_{y,F} + \\ + (k_{M|31} + k_{F|57})u_{x,NCOI} + (k_{M|32} + k_{F|58})u_{y,NCOI} + \\ + (k_{M|17} + k_{M|35})u_{N,MC|7} + (k_{M|18} + k_{M|36})u_{N,MC|8} + (k_{F|71} + k_{F|53})u_{N,FC|1} + (k_{F|72} + k_{F|54})u_{N,FC|2} + \\ + \sum_{i=5}^6 k_{M|1i}u_{N,MC|i} + \sum_{i=7}^8 k_{M|3i}u_{N,MB|i} + \sum_{i=2}^3 k_{F|7i}u_{N,FC|i} + \sum_{i=1}^2 k_{F|5i}u_{N,FB|i} = 0 \\ (k_{e,M|21} + k_{e,M|43} + k_{e,F|87} + k_{e,F|65})u_{x,MCT} + (k_{e,M|22} + k_{e,M|44} + k_{e,F|88} + k_{e,F|66})u_{y,MCT} + \\ + k_{e,M|23}u_{x,M} + k_{e,M|24}u_{y,M} + k_{e,F|85}u_{x,F} + k_{e,F|86}u_{y,F} + \\ + (k_{M|41} + k_{F|67})u_{x,NCOI} + (k_{M|42} + k_{F|68})u_{y,NCOI} + \\ + (k_{M|27} + k_{M|45})u_{N,MC|7} + (k_{M|28} + k_{M|46})u_{N,MC|8} + (k_{F|81} + k_{F|63})u_{N,FC|1} + (k_{F|82} + k_{F|64})u_{N,FC|2} + \\ + \sum_{i=2}^3 k_{F|8i}u_{N,FC|i} + \sum_{i=1}^2 k_{F|6i}u_{N,FB|i} + \sum_{i=5}^6 k_{M|2i}u_{N,MC|i} + \sum_{i=7}^8 k_{M|4i}u_{N,MB|i} = 0 \end{cases}. \quad (\text{A.19})$$

Solving the system of two equations and observing that $u_{x,F}, u_{y,F} \sim 0$ for a stiffer inclusion as a fiber in a polymeric composite, we can express $u_{x,MCT}$ as a function of u_x and u_y (see Eq. (A.14)) as

$$\begin{aligned}
& \left[(k_{e,M|21} + k_{e,M|43} + k_{e,F|87} + k_{e,F|65}) + \frac{k_{e,M|11} + k_{e,M|33} + k_{e,F|77} + k_{e,F|55}}{k_{e,M|12} + k_{e,M|34} + k_{e,F|78} + k_{e,F|56}} (k_{e,M|22} + k_{e,M|44} + k_{e,F|88} + k_{e,F|66}) \right] u_{x,MCT} + \\
& + \left(k_{e,M|23} - \frac{k_{e,M|22} + k_{e,M|44} + k_{e,F|88} + k_{e,F|66}}{k_{e,M|12} + k_{e,M|34} + k_{e,F|78} + k_{e,F|56}} k_{e,M|13} \right) u_x + \\
& + \left(k_{e,M|24} - \frac{k_{e,M|22} + k_{e,M|44} + k_{e,F|88} + k_{e,F|66}}{k_{e,M|12} + k_{e,M|34} + k_{e,F|78} + k_{e,F|56}} k_{e,M|14} \right) u_y + \\
& + \left(k_{e,M|23} + k_{e,F|85} - \frac{k_{e,M|22} + k_{e,M|44} + k_{e,F|88} + k_{e,F|66}}{k_{e,M|12} + k_{e,M|34} + k_{e,F|78} + k_{e,F|56}} (k_{e,M|13} + k_{e,M|75}) \right) \underline{u_{x,F}} \approx 0 + \\
& + \left(k_{e,M|24} + k_{e,F|86} - \frac{k_{e,M|22} + k_{e,M|44} + k_{e,F|88} + k_{e,F|66}}{k_{e,M|12} + k_{e,M|34} + k_{e,F|78} + k_{e,F|56}} (k_{e,M|14} + k_{e,M|76}) \right) \underline{u_{y,F}} \approx 0 + \\
& + \left[(k_{M|41} + k_{F|67}) - \frac{k_{e,M|22} + k_{e,M|44} + k_{e,F|88} + k_{e,F|66}}{k_{e,M|12} + k_{e,M|34} + k_{e,F|78} + k_{e,F|56}} (k_{M|31} + k_{F|57}) \right] u_{x,NCOI} + \\
& + \left[(k_{M|42} + k_{F|68}) - \frac{k_{e,M|22} + k_{e,M|44} + k_{e,F|88} + k_{e,F|66}}{k_{e,M|12} + k_{e,M|34} + k_{e,F|78} + k_{e,F|56}} (k_{M|32} + k_{F|58}) \right] u_{y,NCOI} + \\
& + (k_{M|27} + k_{M|45}) u_{N,MC|7} + (k_{M|28} + k_{M|46}) u_{N,MC|8} + (k_{F|81} + k_{F|63}) u_{N,FC|1} + (k_{F|82} + k_{F|64}) u_{N,FC|2} + \\
& - \frac{k_{e,M|22} + k_{e,M|44} + k_{e,F|88} + k_{e,F|66}}{k_{e,M|12} + k_{e,M|34} + k_{e,F|78} + k_{e,F|56}} [(k_{M|17} + k_{M|35}) u_{N,MC|7} + (k_{M|18} + k_{M|36}) u_{N,MC|8}] + \\
& - \frac{k_{e,M|22} + k_{e,M|44} + k_{e,F|88} + k_{e,F|66}}{k_{e,M|12} + k_{e,M|34} + k_{e,F|78} + k_{e,F|56}} [(k_{F|71} + k_{F|53}) u_{N,FC|1} + (k_{F|72} + k_{F|54}) u_{N,FC|2}] \\
& + \sum_{i=2}^3 k_{F|8i} u_{N,FC|i} + \sum_{i=1}^2 k_{F|6i} u_{N,FB|i} + \sum_{i=5}^6 k_{M|2i} u_{N,MC|i} + \sum_{i=7}^8 k_{M|4i} u_{N,MB|i} + \\
& - \frac{\sum_{i=5}^6 k_{M|1i} u_{N,MC|i} + \sum_{i=7}^8 k_{M|3i} u_{N,MB|i} + \sum_{i=2}^3 k_{F|7i} u_{N,FC|i} + \sum_{i=1}^2 k_{F|5i} u_{N,FB|i}}{k_{e,M|12} + k_{e,M|34} + k_{e,F|78} + k_{e,F|56}} = 0,
\end{aligned} \tag{A.20}$$

while the reaction forces at the crack tip can be expressed as

$$\begin{cases}
F_{x,CT} = R_{x,FCT} = \\
= (k_{e,F|77} + k_{e,F|55}) u_{x,FCT} + (k_{e,F|78} + k_{e,F|56}) u_{y,FCT} + \\
+ k_{e,F|75} \underline{u_{x,F}} \approx 0 + k_{e,F|76} \underline{u_{y,F}} \approx 0 + \\
+ \sum_{i=1}^4 k_{e,F|7i} u_{N,FC|i} + \sum_{i=1, i \neq (5,6)}^8 k_{e,F|5i} u_{N,FB|i} \\
F_{y,CT} = R_{y,FCT} = \\
= (k_{e,F|87} + k_{e,F|65}) u_{x,FCT} + (k_{e,F|88} + k_{e,F|66}) u_{y,FCT} + \\
+ k_{e,F|85} \underline{u_{x,F}} \approx 0 + k_{e,F|86} \underline{u_{y,F}} \approx 0 + \\
+ \sum_{i=1}^4 k_{e,F|8i} u_{N,FC|i} + \sum_{i=1, i \neq (5,6)}^8 k_{e,F|6i} u_{N,FB|i}
\end{cases} \tag{A.21}$$

Substituting Eq. (A.18) in Eqs. (A.19)–(A.21) and solving, we obtain an expression of the form

$$\begin{cases}
F_{x,CT} = K_{xx} u_x + K_{xy} u_y \\
+ \sum_{i=1}^4 K_{FC,x|i} u_{N,FC|i} + \sum_{i=1, i \neq (3,4,5,6)}^8 K_{FB,x|i} u_{N,FB|i} \\
+ \sum_{i=5}^8 K_{FC,x|i} u_{N,MC|i} + \sum_{i=7}^8 K_{MB,x|i} u_{N,FB|i} \\
F_{y,CT} = K_{yx} u_x + K_{yy} u_y \\
+ \sum_{i=1}^4 K_{FC,y|i} u_{N,FC|i} + \sum_{i=1, i \neq (3,4,5,6)}^8 K_{FB,y|i} u_{N,FB|i} \\
+ \sum_{i=5}^8 K_{FC,y|i} u_{N,MC|i} + \sum_{i=7}^8 K_{MB,y|i} u_{N,FB|i}
\end{cases}, \tag{A.22}$$

which can be reformulated synthetically as

$$\begin{cases}
F_{x,CT} = K_{xx} u_x + K_{xy} u_y + \tilde{F}_x \\
F_{y,CT} = K_{yx} u_x + K_{yy} u_y + \tilde{F}_y
\end{cases}, \tag{A.23}$$

where \tilde{F}_x and \tilde{F}_y represent the influence of the FE solution through the nodes of the elements sharing the crack tip that do not belong to any of the phase interfaces, i.e. the nodes of the elements sharing the crack tip that belong to the bulk of each phase.

Appendix B. Expression of $T_{\Rightarrow pq}$ for quadrilateral elements with or without singularity

The expression of $T_{\Rightarrow pq}$ for quadrilateral elements with or without singularity is

$$\begin{aligned}
\underline{\underline{T}}_{pq} &= \begin{cases} \underline{I} & \text{for } p = q < 2 \\ \underline{0} & \text{otherwise} \end{cases} \\
&\quad \times \text{ for } 1^{\text{st}} \text{ order quadrilateral elements} \\
&= \begin{cases} \underline{I} & \text{for } p = q < 3 \\ \underline{0} & \text{otherwise} \end{cases} \\
&\quad \times \text{ for } 2^{\text{nd}} \text{ order quadrilateral elements} \\
&= \begin{cases} \underline{I} & \text{for } p = q < 4 \\ \underline{0} & \text{otherwise} \end{cases} \quad \text{for } 3^{\text{rd}} \text{ order quadrilateral elements} \\
&= \begin{cases} \left(14 - \frac{33\pi}{8}\right) \underline{I} & \text{for } p = 1, q = 1 \\ \left(-52 + \frac{33\pi}{2}\right) \underline{I} & \text{for } p = 1, q = 2 \\ \left(17 - \frac{21\pi}{4}\right) \underline{I} & \text{for } p = 2, q = 1 \\ \left(-\frac{7}{2} + \frac{21\pi}{16}\right) \underline{I} & \text{for } p = 2, q = 2 \\ \left(8 - \frac{21\pi}{8}\right) \underline{I} & \text{for } p = 1, q = 3 \\ \left(-32 + \frac{21\pi}{2}\right) \underline{I} & \text{for } p = 2, q = 3 \\ \underline{0} & \text{otherwise} \end{cases} \\
&\quad \times \text{ for } 2^{\text{nd}} \text{ order quarter – point quadrilateral elements} \\
&= \begin{cases} \left(-11187 + \frac{7155\pi}{2}\right) \underline{I} & \text{for } p = 1, q = 1 \\ \left(38556 - \frac{24543\pi}{2}\right) \underline{I} & \text{for } p = 1, q = 2 \\ \left(-53055 + \frac{33777\pi}{2}\right) \underline{I} & \text{for } p = 1, q = 3 \\ \left(\frac{11396}{3} - \frac{9575\pi}{8}\right) \underline{I} & \text{for } p = 2, q = 1 \\ \left(-12936 + \frac{33003\pi}{8}\right) \underline{I} & \text{for } p = 2, q = 2 \\ \left(17988 - \frac{45837\pi}{8}\right) \underline{I} & \text{for } p = 2, q = 3 \\ \left(-\frac{8453}{3} + \frac{3595\pi}{4}\right) \underline{I} & \text{for } p = 3, q = 1 \\ \left(9804 - \frac{12411\pi}{4}\right) \underline{I} & \text{for } p = 3, q = 2 \\ \left(-13587 + \frac{17289\pi}{4}\right) \underline{I} & \text{for } p = 3, q = 3 \\ \left(6948 - \frac{17685\pi}{8}\right) \underline{I} & \text{for } p = 1, q = 4 \\ \left(-23976 + \frac{60993\pi}{8}\right) \underline{I} & \text{for } p = 2, q = 4 \\ \left(33372 - \frac{84807\pi}{8}\right) \underline{I} & \text{for } p = 3, q = 4 \\ \underline{0} & \text{otherwise} \end{cases} \\
&\quad \times \text{ for } 3^{\text{rd}} \text{ order quarter – point quadrilateral elements}
\end{aligned} \tag{B.1}$$

where \underline{I} is the identity matrix.

References

- [1] M. Comninou, An overview of interface cracks, *Eng. Fract. Mech.* 37 (1) (1990) 197–208, [https://doi.org/10.1016/0013-7944\(90\)90343-f](https://doi.org/10.1016/0013-7944(90)90343-f).
- [2] D. Hills, J. Barber, Interface cracks, *Int. J. Mech. Sci.* 35 (1) (1993) 27–37, [https://doi.org/10.1016/0020-7403\(93\)90062-y](https://doi.org/10.1016/0020-7403(93)90062-y).
- [3] M.L. Williams, The stresses around a fault or crack in dissimilar media, *Bull. Seismol. Soc. Am.* 49 (2) (1959) 199.
- [4] J. Dundurs, Discussion: edge-bonded dissimilar orthogonal elastic wedges under normal and shear loading (Bogy, D. B., 1968, *ASME J. Appl. Mech.*, 35, pp. 460–466), *J. Appl. Mech.* 36 (3) (1969) 650, <https://doi.org/10.1115/1.3564739>.
- [5] F. Erdogan, Stress distribution in a nonhomogeneous elastic plane with cracks, *J. Appl. Mech.* 30 (2) (1963) 232, <https://doi.org/10.1115/1.3636517>.
- [6] A.H. England, A crack between dissimilar media, *J. Appl. Mech.* 32 (2) (1965) 400, <https://doi.org/10.1115/1.3625813>.
- [7] B. Malyshev, R. Salganik, The strength of adhesive joints using the theory of cracks, *Int. J. Fract. Mech.* 11 (2) (1965), <https://doi.org/10.1007/bf00186749>, <https://doi.org/10.1007/bf00186749>.
- [8] M. Comninou, The interface crack, *J. Appl. Mech.* 44 (4) (1977) 631, <https://doi.org/10.1115/1.3424148>, <https://doi.org/10.1115/1.3424148>.
- [9] A.H. England, An arc crack around a circular elastic inclusion, *J. Appl. Mech.* 33 (3) (1966) 637, <https://doi.org/10.1115/1.3625132>.
- [10] A. Perlman, G. Sih, Elastostatic problems of curvilinear cracks in bonded dissimilar materials, *Int. J. Eng. Sci.* 5 (11) (1967) 845–867, [https://doi.org/10.1016/0020-7225\(67\)90009-2](https://doi.org/10.1016/0020-7225(67)90009-2).
- [11] M. Toya, A crack along the interface of a circular inclusion embedded in an infinite solid, *J. Mech. Phys. Solids* 22 (5) (1974) 325–348, [https://doi.org/10.1016/0022-5096\(74\)90002-7](https://doi.org/10.1016/0022-5096(74)90002-7).
- [12] F. Pars, J.C. Cao, J. Varna, The fiber-matrix interface crack a numerical analysis using boundary elements, *Int. J. Fract.* 82 (1) (1996) 11–29, <https://doi.org/10.1007/bf00017861>.
- [13] G.R. Irwin, *Fracture*, in: *Elasticity and Plasticity/Elastizität und Plastizität*, Springer Berlin Heidelberg, 1958, pp. 551–590, https://doi.org/10.1007/978-3-642-45887-3_5.
- [14] J.C.D. Cao, F. Pars, On stress singularities induced by the discretization in curved receding contact surfaces: a bem analysis, *Int. J. Numer. Methods Eng.* 40 (12) (1997) 2301–2320, [https://doi.org/10.1002/\(sici\)1097-0207\(19970630\)40:12<2301::aid-nme166>3.0.co;2-8](https://doi.org/10.1002/(sici)1097-0207(19970630)40:12<2301::aid-nme166>3.0.co;2-8).
- [15] J. Varna, F. Pars, J.C. Cao, The effect of crack-face contact on fiber/matrix debonding in transverse tensile loading, *Compos. Sci. Technol.* 57 (5) (1997) 523–532, [https://doi.org/10.1016/S0266-3538\(96\)00175-3](https://doi.org/10.1016/S0266-3538(96)00175-3).
- [16] F. Pars, E. Correa, V. Manti, Kinking of transversal interface cracks between fiber and matrix, *J. Appl. Mech.* 74 (4) (2007) 703, <https://doi.org/10.1115/1.2711220>.
- [17] E. Correa, E. Gamstedt, F. Pars, V. Manti, Effects of the presence of compression in transverse cyclic loading on fibrematrix debonding in unidirectional composite plies, *Compos. Part A Appl. Sci. Manuf.* 38 (11) (2007) 2260–2269, <https://doi.org/10.1016/j.compositesa.2006.11.002>.
- [18] E. Correa, V. Manti, F. Pars, Effect of thermal residual stresses on matrix failure under transverse tension at micromechanical level: a numerical and experimental analysis, *Compos. Sci. Technol.* 71 (5) (2011) 622–629, <https://doi.org/10.1016/j.compscitech.2010.12.027>.
- [19] E. Correa, F. Pars, V. Manti, Effect of the presence of a secondary transverse load on the inter-fibre failure under tension, *Eng. Fract. Mech.* 103 (2013) 174–189, <https://doi.org/10.1016/j.engfractmech.2013.02.026>.
- [20] E. Correa, F. Pars, V. Manti, Effect of a secondary transverse load on the inter-fibre failure under compression, *Compos. Part B Eng.* 65 (2014) 57–68, <https://doi.org/10.1016/j.compositesb.2014.01.005>.
- [21] C. Sandino, E. Correa, F. Pars, Numerical analysis of the influence of a nearby fibre on the interface crack growth in composites under transverse tensile load, *Eng. Fract. Mech.* 168 (2016) 58–75, <https://doi.org/10.1016/j.engfractmech.2016.01.022>.
- [22] C. Sandino, E. Correa, F. Pars, Interface crack growth under transverse compression: nearby fibre effect, in: *Proceeding of the 18th European Conference on Composite Materials (ECCM-18)*, 2018.
- [23] L. Zhuang, A. Pupurs, J. Varna, R. Talreja, Z. Ayadi, Effects of inter-fiber spacing on fiber-matrix debond crack growth in unidirectional composites under transverse loading, *Compos. Part A Appl. Sci. Manuf.* 109 (2018) 463–471, <https://doi.org/10.1016/j.compositesa.2018.03.031>.
- [24] J. Varna, L.Q. Zhuang, A. Pupurs, Z. Ayadi, Growth and interaction of debonds in local clusters of fibers in unidirectional composites during transverse loading, *Key Eng. Mater.* 754 (2017) 63–66, <https://doi.org/10.4028/www.scientific.net/kem.754.63>.
- [25] L. Zhuang, R. Talreja, J. Varna, Transverse crack formation in unidirectional composites by linking of fibre/matrix debond cracks, *Compos. Part A Appl. Sci. Manuf.* 107 (2018) 294–303, <https://doi.org/10.1016/j.compositesa.2018.01.013>.
- [26] E. Rybicki, M. Kanninen, A finite element calculation of stress intensity factors by a modified crack closure integral, *Eng. Fract. Mech.* 9 (4) (1977) 931–938, [https://doi.org/10.1016/0013-7944\(77\)90013-3](https://doi.org/10.1016/0013-7944(77)90013-3).
- [27] R. Krueger, Virtual crack closure technique: history, approach, and applications, *Appl. Mech. Rev.* 57 (2) (2004) 109, <https://doi.org/10.1115/1.1595677>.
- [28] R. Krueger, K.N. Shivakumar, I.S. Raju, Fracture mechanics analyses for interface crack problems - a review, in: *54th AIAA/ASME/ASCE/AHS/ASC Structures, Structural Dynamics, and Materials Conference*, American Institute of Aeronautics and Astronautics, 2013, <https://doi.org/10.2514/6.2013-1476>.
- [29] C. Sun, C. Jih, On strain energy release rates for interfacial cracks in bi-material media, *Eng. Fract. Mech.* 28 (1) (1987) 13–20, [https://doi.org/10.1016/0013-7944\(87\)90115-9](https://doi.org/10.1016/0013-7944(87)90115-9).
- [30] C. Sun, M. Manoharan, Strain energy release rates of an interfacial crack between two orthotropic solids, *J. Compos. Mater.* 23 (5) (1989) 460–478, <https://doi.org/10.1177/002199838902300503>.
- [31] M. Manoharan, C. Sun, Strain energy release rates of an interfacial crack between two anisotropic solids under uniform axial strain, *Compos. Sci. Technol.* 39 (2) (1990) 99–116, [https://doi.org/10.1016/0266-3538\(90\)90049-b](https://doi.org/10.1016/0266-3538(90)90049-b).
- [32] I. Raju, J. Crews, M. Aminpour, Convergence of strain energy release rate components for edge-delaminated composite laminates, *Eng. Fract. Mech.* 30 (3) (1988) 383–396, [https://doi.org/10.1016/0013-7944\(88\)90196-8](https://doi.org/10.1016/0013-7944(88)90196-8).
- [33] E. Glaessen, W. Riddell, I. Raju, Effect of shear deformation and continuity on delamination modeling with plate elements, in: *39th AIAA/ASME/ASCE/AHS/ASC Structures, Structural Dynamics, and Materials Conference and Exhibit*, American Institute of Aeronautics and Astronautics, 1998, <https://doi.org/10.2514/6.1998-2023>.
- [34] A. Agrawal, A.M. Karlsson, Obtaining mode mixity for a bimaterial interface crack using the virtual crack closure technique, *Int. J. Fract.* 141 (12) (2006) 75–98, <https://doi.org/10.1007/s10704-006-0069-4>.
- [35] S. Wang, C. Harvey, L. Guan, Partition of mixed modes in layered isotropic double cantilever beams with non-rigid cohesive interfaces, *Eng. Fract. Mech.* 111 (2013) 1–25, <https://doi.org/10.1016/j.engfractmech.2013.09.005>.
- [36] Simulia, Providence, RI, USA, ABAQUS/Standard User's Manual, 2012, Version 6.12.
- [37] P.S. Valvo, A revised virtual crack closure technique for physically consistent fracture mode partitioning, *Int. J. Fract.* 173 (1) (2011) 1–20, <https://doi.org/10.1007/s10704-011-9658-y>.
- [38] P.S. Valvo, A further step towards a physically consistent virtual crack closure technique, *Int. J. Fract.* 192 (2) (2015) 235–244, <https://doi.org/10.1007/s10704-015-0007-4>.
- [39] G.R. Irwin, Analysis of stresses and strains near the end of a crack traversing a plate, *J. Appl. Mech. - Trans. ASME E24* (1957) 351–369.
- [40] I. Raju, Calculation of strain-energy release rates with higher order and singular finite elements, *Eng. Fract. Mech.* 28 (3) (1987) 251–274, [https://doi.org/10.1016/0013-7944\(87\)90220-7](https://doi.org/10.1016/0013-7944(87)90220-7).
- [41] W.T. Chow, S.N. Atluri, Finite element calculation of stress intensity factors for interfacial crack using virtual crack closure integral, *Comput. Mech.* 16 (6) (1995) 417–425, <https://doi.org/10.1007/bf00370563>.